8. MULTI CRITERIA SHAPE CONTROL

Technology makes it possible for people to gain control over everything, except over technology. - John Tudor.

8.1 The need for higher level shape control

The "higher level" SC refers to the use of quantities such as slopes and curvatures to describe or measure the "shape", in contrast to using displacements only (DBSC). In the previous chapter, an intuitive / heuristic SC algorithm was developed that had incorporated elements of the SPEC method, evolutionary strategies and artificial neural networks. The BVD algorithm iteratively builds up the voltage magnitudes of each potentially active patch, thus resulting in a final voltage distribution. Like many other SC work, BVD is a DBSC algorithm based on minimizing transverse displacements between the desired shape and the actual shape of the structure. The results in Chap. 7 have shown that DBSC is basically effective, but there are limitations. These limitations have led to the present development of multi-criteria shape control (MCSC) which propose to use both the slopes and displacements. This is then extended to using curvatures and displacements. Results using MCSC will show improvements over the traditional DBSC techniques.

The investigations in Chap. 7 have revealed many issues that need to be considered when doing SC. It was established that for better shape controllability the actuators should be smaller discrete patches instead of one single layer. This enables the inducement of multi-modal shapes and multiple curvatures; essentially, more independent discrete patches mean the ability to conform to more complex shapes. Therefore the investigations from now on will involve structures with actuator patches rather than continuous layers. Recall, from Chap. 7, that achieving the exact desired shape is often impossible with the exception of the simplest cases, hence the goal of minimizing the difference between the actual and desired shape.

One consequence of using discrete patches in SC that was not mentioned in the previous chapter, can be seen quite evidently in the 3-dimensional oblique view of the transverse displacement plots of the structures (e.g. Fig. 7.11b,c,d). In the aforementioned plots, the cantilever structure of §7.5.3 with 15 actuator patches was made to twist according to the

function given by Eq. (7.18). Part of the structure, ($y>0$), needs to deflect upward, while the other part, ($y<0$), needs to deflect downward. In the attempt to conform to the desired twist shape, each actuator produces independent actuation such that the actual shape will globally be very similar to the desired shape. The side-effect of the localized influence of the actuators, which was not mentioned before, is the bumpiness or unevenness of the transverse displacements. Bear in mind that in the 3-D plots, the transverse deflection has been magnified compared to the in-plane dimensions, (the maximum point being 10% of the full z-scale of the plotting screen). This bumpiness has been tested and was found to be independent of the mesh size - i.e. the bumpiness still exists at the patches no matter what FE mesh was used - thus ruling out numerical causes.

To the best of this author's knowledge, this phenomenon has not been reported in the literature in the field of SC with patch actuators. It is believed that these bumpy regions are due to the limitation of DBSC in actuating a structure with discrete actuator patches. The effect is especially pronounced when adjacent actuator patches have quite different voltages. This effect does more than produce an unaesthetic 3-D plot of the transverse displacement - its subsequent effect is likely to correspond to localized stress concentrations around the active patches, as the structure is being forced to conform to the desired shape. Needless to say there is good reason for reducing these bumpiness and at the same time reducing the stress concentrations. The results obtained in this chapter do show that the actual stress concentrations are less when the unevenness of the transverse displacement is reduced.

The novel contribution of this chapter is to utilize "slope" as the additional criteria for MCSC, (some references to "slope" from now on may have a counterpart in "curvature" which will be developed later). The reason for choosing slope and curvature to perform more accurate SC is driven by the desire to "smooth" the actuated structure, and it is believed that the use of these two variables could achieve this goal because they too are geometrical attributes of the shape of the structure. Several of the generic methods such as Linear Least Squares (LLS) and Simulated Annealing (SA) were used after appropriate modifications were made to them. The results, discussed later, show that they are partially effective but there seems to be certain aspects that can still be improved upon.

This led to the development of the algorithm called Perturbation Buildup Voltage Distribution (PBVD), (Chee et. al. 2000a), which is an iterative algorithm with a concept similar to BVD. Initially, displacement shape control based on a LLS fit is performed on the structure. The result is a structure with some bumpiness and this is taken as the initial configuration for PBVD. In PBVD, slope is regarded as the fine-tuning criteria to smoothen the structure. In the

iterative process, the voltage on the patches are perturbed and build up based on a cost function determined by the slope.

The performance of PBVD as a shape control algorithm will be investigated using some new examples, in particular results showing stresses. There are not many examples in this category of shape control using a high order control criteria, such as slope, and its effects on stresses, hence the results here may be useful benchmarks for future investigations. The quality of the solution or the algorithm can be assessed by how close the actual shape matches the desired shape - thus in the objective of SSC, verification can be performed without third party results.

8.2 Slopes and Curvatures in MCSC

8.2.1. Definition of Slope in Slope Displacement Shape Control and its Objective Function

In Chap. 7 the only SC criterion used is based on the mid-plane or the reference transverse displacement *w*. Although this provides reasonable results, this section will improve on this type of SC by using an additional criteria which is the transverse slopes of the structure. The use of displacements and slope criteria only, is hereon called *Slope Displacement Shape Control* (SDSC). The general problem is similar to that defined in §7.1.5., in which the voltage distribution is sought. The slopes with respect to the *x-y* plane are defined as Eq. (8.1) in the FE formulation, where the $[u^c]$ is the contracted displacement vector of Eq. (3.2) which represent the variable *w* in this case. The superscript(^{c}) on other variables indicate the contracted notation for the mechanical shape function matrix $[N_u^c]$ and nodal displacement vector $[u_e^c]$ respectively.

$$\begin{bmatrix} S_x \\ S_y \end{bmatrix} = \begin{bmatrix} \frac{\partial}{\partial x} \\ \frac{\partial}{\partial y} \end{bmatrix} [w] = [D_S(x,y)][u^c] = [D_S(x,y)][N_u^c(\xi,\eta)][u_e^c] \tag{8.1}$$

As with the displacement/voltage linearity (§7.1.2), there exists a linear relationship between the voltage and slope due to the linear model of the constitutive properties and the governing equations. Thus the slopes at any points (specified later), can be directly related to the applied patch voltages by the influence coefficient (IC) matrices obtained by FEA. This can be expressed in Eq. (8.2) by using the IC of slopes, $[C^{Sx}, C^{Sy}]$, which can be determined in a similar manner to its displacement counterpart in Eq. (7.1). This reduces computational time significantly when new values are calculated because there is no need to reiterate the entire FE process for slope calculations.

$$S_{x\,i} = C_{ik}^{Sx}\phi_k; \qquad S_{y\,i} = C_{ik}^{Sy}\phi_k \tag{8.2}$$

where $i = 1....$Total Number of slope points considered & $k = 1....Np$ (Total number of active patches).

When the voltage is perturbed by a small amount $d\phi_k = dV$ at patch k only, from the base voltage configuration $\{\phi^o\}$, then the slopes of the perturbed structure is given by Eq. (8.3), where superscript o = quantities in base configuration.

$$\{S_x\} = \{S_x^o\} + \{C^{Sx}\}_k d\phi_k \quad ; \quad \{S_y\} = \{S_y^o\} + \{C^{Sy}\}_k d\phi_k \tag{8.3}$$

In addition to the objective function or measure for the displacement, *LSw*, defined in Eq. (7.2), the two new measures of *slope* conformity between the actual and desired shapes are *LSSx* and *LSSy* given by Eq. (8.4).

$$LSSx = \frac{\sum_{i=1}^{N_S} (S_{x\,i} - S_{x\,i}^d)^2}{N_S \times Max_{\forall i}(|S_{x\,i}^d|)^2} \quad ; \quad LSSy = \frac{\sum_{i=1}^{N_S} (S_{y\,i} - S_{y\,i}^d)^2}{N_S \times Max_{\forall i}(|S_{y\,i}^d|)^2} \tag{8.4}$$

where N_S = total number of points where slope is calculated (see §8.2.3).

In SDSC, the aim is to minimize the displacement as well as the slopes as represented by *LSw* and *LSSx, LSSy*. Depending on the optimization algorithms used, these 3 measures can be optimized separately or they can be coupled into one single objective function such as *LSobj*, which is defined as the sum of the three displacements and slopes measures, Eq. (8.5). An extra set of weights $\{\alpha^w, \alpha^{Sx}, \alpha^{Sy}\}$ are also attached to each of the three criterion to allow for a limited amount of user controllability over the optimization process.

$$LSobj = \alpha^w LSw + \alpha^{Sx} LSSx + \alpha^{Sy} LSSy \tag{8.5}$$

8.2.2. Definition of Curvature in Curvature Displacement Shape Control and its Objective Function

In addition to slopes, the *curvatures* will also be used as an additional criteria in shape control. The use of displacement and curvature criteria only, is hereon called *Curvature Displacement Shape Control* (CDSC). The curvatures that are to be used as the SC criteria are defined as the "global" curvatures (*gK*) as used by Koconis et. al. (1994a) and Kollar (1990), which is suitable for structures that include transverse shear deformations. Hence the global curvatures are defined using the first order terms of the third order displacement field, Eq. (3.1). This definition differs from the usual definition of curvature as the second derivative of the transverse displacements, which is described here as the "reference" curvature (*rK*) because that

uses the mid-plane transverse displacement *w*. Both types of curvatures are shown in Eq. (8.6). The difference in magnitude between these two curvatures are the magnitudes of the transverse shear strains. However, in this thesis, only the set of *gK* curvatures will be used as the SC criteria, and the prefix '*g*' in *gK* will be dropped.

$$gK_{xx} = -\frac{\partial}{\partial x}\psi_x \quad ; \qquad gK_{yy} = -\frac{\partial}{\partial y}\psi_y \quad ; \qquad gK_{xy} = -\frac{\partial}{\partial x}\psi_y - \frac{\partial}{\partial y}\psi_x$$
$$rK_{xx} = \frac{\partial^2}{\partial x^2}w \quad ; \qquad rK_{yy} = \frac{\partial^2}{\partial y^2}w \quad ; \qquad rK_{xy} = 2\frac{\partial^2}{\partial x \partial y}w \tag{8.6}$$

In FE, the curvatures are expressed using only 2 of the 11 nodal coordinates. Equation (8.7) shows its FE form using a contracted (^{c}) nodal vector notation, where $[u^c]$ is the contracted displacement vector of Eq. (3.2) with variables ψ_x & ψ_y only; and the mechanical shape function matrix $[N_u^c]$ and nodal displacement vector $[u_e^c]$ respectively.

$$\begin{bmatrix} K_{xx} \\ K_{yy} \\ K_{xy} \end{bmatrix} = \begin{bmatrix} \frac{\partial}{\partial x} & 0 \\ 0 & \frac{\partial}{\partial y} \\ \frac{\partial}{\partial y} & \frac{\partial}{\partial x} \end{bmatrix} \begin{bmatrix} \psi_x \\ \psi_y \end{bmatrix} = [D_K(x,y)][u^c] = [D_K(x,y)][N_u^c(\xi,\eta)][u_e^c] \tag{8.7}$$

Again, due to the linearity of the mathematical model, there exist a linear relationship between curvatures and the applied voltage. This linearity holds for nodal curvatures as well as any curvatures calculated using these nodal values, e.g. curvature-area integral used later on. Consequently, the curvatures can also be related to the voltages applied on the actuator patches, once their influence coefficients, C^K, are determined, see Eq. (8.8).

$$K_{xx\ i} = C_{ik}^{Kxx}\phi_k \quad ; \qquad K_{yy\ i} = C_{ik}^{Kyy}\phi_k \quad ; \qquad K_{xy\ i} = C_{ik}^{Kxy}\phi_k \tag{8.8}$$

where *i =1*....Total Number of points considered & *k = 1....Np* (Total number of active patches).

When the voltage is perturbed by a small amount $d\phi_k = dV$ at patch *k* only, from the base voltage configuration $\{\phi^o\}$ then the curvatures of the perturbed structure is given by Eq. (8.9), where superscript *o* = quantities in base configuration.

$$\{K_{xx}\} = \{K_{xx}^o\} + \{C^{Kxx}\}_k d\phi_k \quad ; \qquad \{K_{yy}\} = \{K_{yy}^o\} + \{C^{Kyy}\}_k d\phi_k$$
$$\{K_{xy}\} = \{K_{xy}^o\} + \{C^{Kxy}\}_k d\phi_k \tag{8.9}$$

The three new measures of curvature conformity between the actual and desired shapes are *LSKxx, LSKyy* and *LSKxy* given by Eq. (8.10).

$$LSKxx = \frac{\sum_{i=1}^{N_K} (K_{xx\ i} - K_{xx\ i}^{d})^2}{N_K \times Max_{\forall i}(|K_{xx\ i}^{d}|)^2} \quad ; \quad LSKyy = \frac{\sum_{i=1}^{N_K} (K_{yy\ i} - K_{yy\ i}^{d})^2}{N_K \times Max_{\forall i}(|K_{yy\ i}^{d}|)^2}$$
$$LSKxy = \frac{\sum_{i=1}^{N_K} (K_{xy\ i} - K_{xy\ i}^{d})^2}{N_K \times Max_{\forall i}(|K_{xy\ i}^{d}|)^2} \tag{8.10}$$

where N_K = total number of points where curvature is calculated (see §8.2.3).

In CDSC, the aim is to minimize the displacement and the curvatures as represented by *LSw* and *LSKxx, LSKyy & LSKxy*. These four measures can be optimized separately or together in one single objective function. Another version of *LSobj*, (previously Eq. (8.5)) can also be defined as the sum of the four displacements and curvature measures in Eq. (8.11). An extra set of weights $\{\alpha^{w}, \alpha^{Kxx}, \alpha^{Kyy}, \alpha^{Kxy}\}$ allow the user to set a limited amount of bias over the criteria to be optimized.

$$LSobj = \alpha^{w} LSw + \alpha^{Kxx} LSKxx + \alpha^{Kyy} LSKyy + \alpha^{Kxy} LSKxy \tag{8.11}$$

8.2.3 A Note on the Points Chosen for Slope & Curvature Evaluation

For the numerical calculations to be presented later, the slopes are calculated at the 4 Gauss points of the element while the curvatures are calculated at the Single Gauss point at the center of each element. Thus $N_S = 4$ in Eq. (8.4) and $N_K = 1$ in Eq. (8.10). The main reason is simply because the program used in this thesis, TODL-FE, uses an 8-node Serendipity element which is able to model a second order or lower order function perfectly. Anything beyond a second order can only be approximated by the 8 node element. This is clearly evident by looking at the 8-node shape functions where the local spatial variables (ξ, η) are at most second order.

Consider the *desired* function *w(x,y)* that is being modeled by the 8 node element, then the 8-node finite element will model it up to a second order function at most, $w(x,y) = O(x^2, y^2)$. All higher order information may be lost. Subsequently, the slopes are of order $O(x^1,y^1)$, and can model any first order or linear function perfectly. The accuracy to represent slopes of second order or higher is not guaranteed. Similarly, the desired curvatures are $O(x^0,y^0)$, which can only represent any constant value function within the element. In some simple cases, it can represent functions of first order or higher, but this is not true for all cases. This can be illustrated from Eq. (8.12) which are the curvature expressions for the 8-node serendipity element, based on the second derivatives of w (where $\{w_n\}$ are the transverse nodal displacements and Δx, Δy the dimensions of the element). For example although K_{xx} is a linear function of η, if the desired K_{xx}

curvature depends on the ξ coordinate too, then the ξ dependence will not be able to be represented in the K_{xx} in Eq. (8.12). However, it would have no problem in modeling constant curvature values.

$$K_{xx} = \frac{4}{\Delta x^2}[\tfrac{1}{2}(1-\eta) \quad (\eta-1) \quad \tfrac{1}{2}(1-\eta) \quad 0 \quad \tfrac{1}{2}(1+\eta) \quad -(1+\eta) \quad \tfrac{1}{2}(1+\eta) \quad 0]\ \{w_n\}$$

$$K_{yy} = \frac{4}{\Delta y^2}[\tfrac{1}{2}(1-\xi) \quad 0 \quad \tfrac{1}{2}(1+\xi) \quad -(\xi+1) \quad \tfrac{1}{2}(1+\xi) \quad 0 \quad \tfrac{1}{2}(1-\xi) \quad (\xi-1)]\ \{w_n\} \qquad (8.12)$$

$$K_{xy} = 2\times\frac{4}{\Delta x\Delta y}[\tfrac{-(2\xi+2\eta-1)}{4} \quad \xi \quad \tfrac{-(2\xi-2\eta+1)}{4} \quad -\eta \quad \tfrac{(2\xi+2\eta+1)}{4} \quad -\xi \quad \tfrac{(2\xi-2\eta-1)}{4} \quad \eta]\ \{w_n\}$$

Hence to be conservative, four Gauss points are chosen for the slopes which allow up to a bilinear variation in the slope within the element. Similarly, one Gauss point is chosen for the curvatures to allow only constant value curvatures in each element. It should be noted here that the initial numerical experiments done in the present research, used several groups of points including nine Gauss points, eight nodal points, four Gauss points and one Gauss point for slopes and curvatures. For those particular tests, it does not appear that the use of different groups of points affect the overall trend of the results significantly.

8.3 Extension of LLS for MCSC

As an initial attempt, MCSC will incorporate all three types of criteria, viz, displacements, slopes and curvatures. The objective function would be a combination of Eq. (8.5) & (8.11) and is given in Eq. (8.13).

$$LSobj = \alpha^{w}LSw + \alpha^{Sx}LSSx + \alpha^{Sy}LSSy + \alpha^{Kxx}LSKxx + \alpha^{Kyy}LSKyy + \alpha^{Kxy}LSKxy \qquad (8.13)$$

Since in this thesis the mathematical model is linear and each of the criterion is linear with respect to the voltage, the most convenient algorithm to use is the LLS method. This is provided there are no two identical actuation response components. Otherwise, there will be a singular matrix. In this simple procedure, all of the criteria are minimized together as in Eq. (8.13), where the weights, α, allow minimal control over which criteria to be minimized. This section extends the LLS method described in §7.2.2. and the general formulation for multi-criteria LLS, now called McLLS, is given by Eq. (8.14) which is another form of Eq. (8.13).

$$\mathscr{E} = \frac{1}{2} \sum_{j=1}^{j=6} \frac{\alpha_i}{\beta_i} (\{\lambda\}_i - \{\lambda^d\}_i)^2$$

$$\begin{aligned}
&\textit{where superscript } d = \textit{desired quantities} \\
&\{\lambda\}_{1,\ldots,6} = \{w\},\{S_x\},\{S_y\},\{K_{xx}\},\{K_{yy}\},\{K_{xy}\} \\
&\alpha_{1,\ldots,6} = \alpha^w,\ \alpha^{Sx},\ \alpha^{Sy},\ \alpha^{Kxx},\ \alpha^{Kyy},\ \alpha^{Kxy} \qquad \ldots\ldots\ldots\ldots\ldots\textit{weights} \\
&\beta_{1,\ldots,6} = Max_{\forall i}(|w^d_i|)^2\ ,\ Max_{\forall i}(|S^d_{x\,i}|)^2\ ,\ Max_{\forall i}(|S^d_{y\,i}|)^2, \\
&Max_{\forall i}(|K^d_{xx\,i}|)^2\ ,\ Max_{\forall i}(|K^d_{yy\,i}|)^2\ ,\ Max_{\forall i}(|K^d_{xy\,i}|)^2 \ \ldots\ldots\ldots\textit{Normalization constants}
\end{aligned} \tag{8.14}$$

The derivation of the solution is analogous to the case for the single variable LLS and since this is a common method, its solution Eq. (8.15), is presented without any further details. The solution of McLLS in terms of the voltage $\{\phi\}$, is expressed using the IC matrices for displacements, slopes and curvatures from Eq. (7.1), (8.2) & (8.8) respectively.

$$\{\phi\} = \left(\sum_{j=1}^{j=6} \frac{\alpha_i}{\beta_i} [C]_i^T [C]_i\right)^{-1} \left(\sum_{j=1}^{j=6} \frac{\alpha_i}{\beta_i} [C]_i^T \{\lambda^d\}_i\right) \tag{8.15}$$

$$\begin{aligned}
&\textit{where } [C]_{1,\ldots,6} = [C^w],\ [C^{Sx}],\ [C^{Sy}],\ [C^{Kxx}],\ [C^{Kyy}]\ [C^{Kxy}] \\
&\ldots\ldots\textit{Influence Coefficient Matrices}
\end{aligned}$$

In practice, the weights can be set to any magnitude but it is recommended to use values in the range of [*0,1*] for ease of comparison.

8.4 Performance of McLLS in MCSC

A series of tests is presented here using McLLS for MCSC that use all three types of criteria - displacements, slopes and curvatures. The goal is to incorporate various combinations of these criteria and determine how to achieve improvement in conforming to the desired shape, viz reducing the bumpiness of the transverse displacements. The initial tests are done using McLLS since this non-iterative method is among the quickest and the goal is also to check the suitability of this method for MCSC. Consider a cantilever structure with 20 actuator patches attached to the surface and with a more elaborate layout than any of the structures considered so far in this thesis. This follows the findings in Chap. 7 that a greater number of discrete actuators allows greater actuation independence and a higher degree of shape controllability. This model differs from the model in Fig 6.5 in that it has two rows on each side of the longitudinal axis of symmetry. This feature would allow the structure to accommodate asymmetrical desired shapes more readily, such as twisting. In general it would allow the investigation of more complex issues in SC.

This cantilever model, which will also be used in other sections, is depicted in Fig. 8.1

and will be referred to as the *Grid* model for convenience. The 20 shaded and numbered regions represent areas designated as active patches. The dimensions of the cantilever plate are length(L) = *150.0mm*, width(C) = *120.0mm* and the thickness of the single-layered Aluminum substrate is *2.0mm*. The gap between the patches and the edge are *5.0mm* and the gap between the patches themselves are *10.0mm*. The active patches are piezoelectric actuators (PIC151), with thickness *0.5mm*, and dimensions *20mm x 20mm* and are attached to the top and bottom layers of the substrate. The material properties are listed under *Aluminum#3* and *PIC151* in Appendix C. For the FE analysis, the structure is divided into 99 elements and 4 layers. In the present case, each patch is modeled by one finite element.

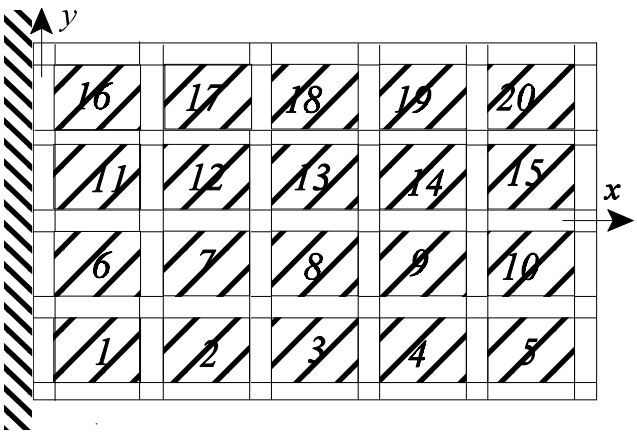

Figure 8.1. Cantilever plate with 99 elements and 20 active patches (not to scale).

The study here focuses on achieving a simple yet quite challenging desired shape. This interesting shape is the *twisted* shape described in Eq. (7.18) that has been used with some examples in Chap. 7. The twisted, wide cantilever example may represent a wing structure that is required to be twisted for aerodynamic purposes.

Table 8.1 Test cases for MCSC using McLLS by variation of weights

Case\Weights	α^{w}	α^{Sx}	α^{Sy}	α^{Kxx}	α^{Kyy}	α^{Kxy}	Figure
1	1	0	0	0	0	0	8.2a
2	0	1	1	0	0	0	8.2b
3	0	0	0	1	1	1	8.2c
4	1	1	1	0	0	0	8.2b
5	1	0	0	1	1	1	8.2c
6	1	1	0	0	0	0	8.2d
7	1	0	1	0	0	0	8.2e
8	1	0	0	1	0	0	8.2c
9	1	0	0	0	1	0	8.2c
10	1	0	0	0	0	1	8.2f
11	1	1	1	1	1	1	8.2c

Recall in §8.1 that the aim to reduce the bumpiness of the resultant structure from DBSC

led to the proposal of MCSC. The series of tests, described in Table 8.1, varies the weights for each of the criteria. In essence, cases 2-11 (Table 8.1) investigates the combinations of various criteria with respect to case 1 which used only displacements as the SC criterion - DBSC. The weights are limited to a value of 0 or 1. In general the weights can have any positive real value, but this test series is only interested in examining some overall major effects. The response to the different weight settings on the actual structure can be seen graphically in the oblique views in Fig 8.2a-8.2f, superimposing the desired shape on the actual shape. Several of the cases responded similarly, so only 6 distinct graphical figures are shown to represent the 11 cases.

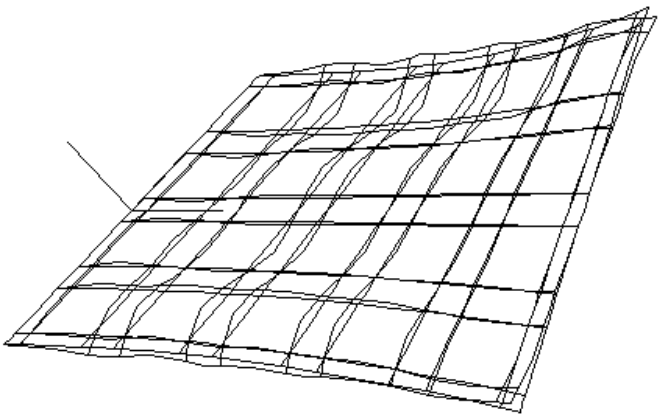

Figure 8.2a. Case 1 - Pure displacement shape control. Oblique view of *desired* shape superimposed on *actual* shape. Unevenness or bumpiness of structure shown.

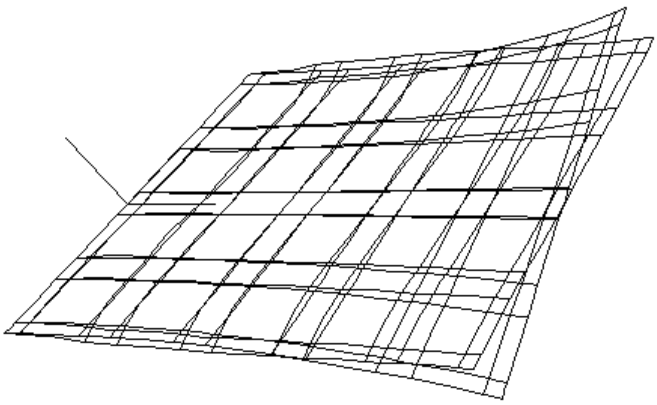

Figure 8.2b. Case 2 - Using slope criteria only. Structure is smoothed but tip diverge. Case 4 has similar response.

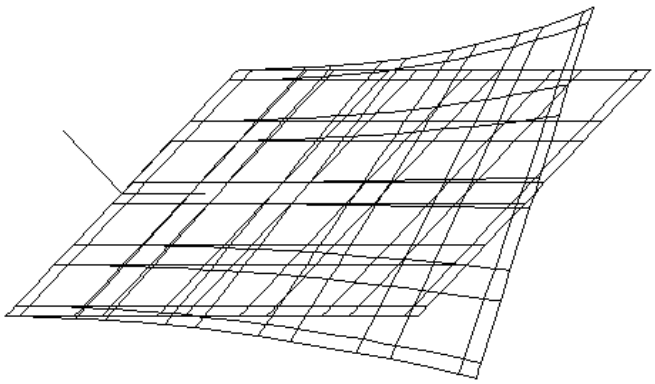

Figure 8.2c. Case 3 - Using curvature criteria only. Structure is smoothed but tip diverge excessively. Cases 5,8,9,11 have similar response.

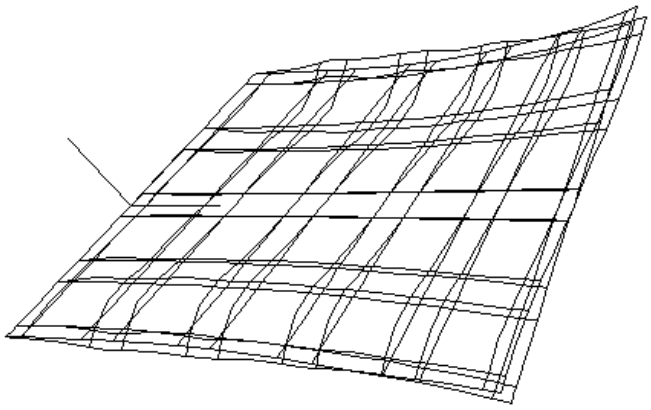

Figure 8.2d. Case 6 - Using *w* and *Sx* criteria only. Central region smoothed but overall displacements conforms less to desired shape.

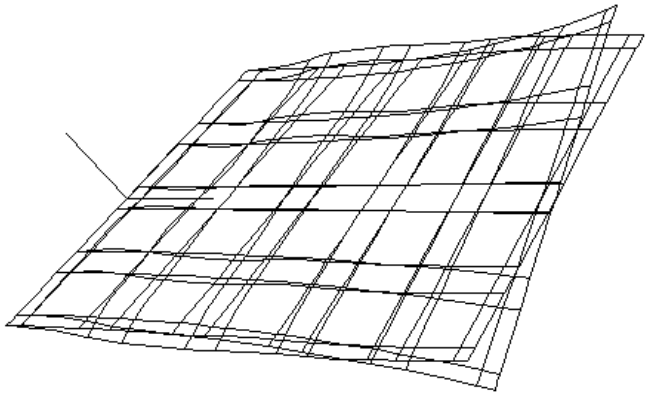

Figure 8.2e. Case 7 - Using *w* and *Sy* criteria only. Structure is smooth but different from desired shape.

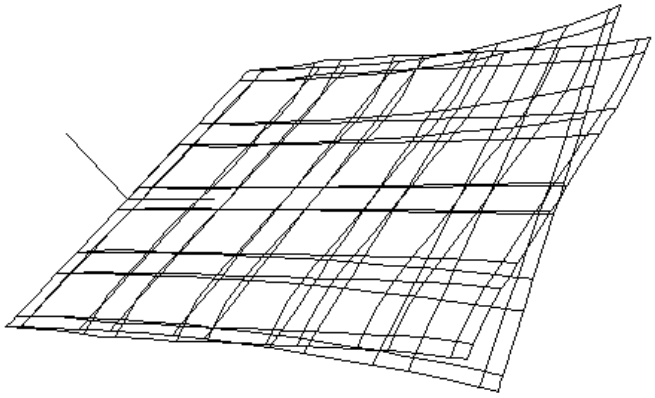

Figure 8.2f. Case 10 - Using *w* and *Kxy* criteria only. Region near wall is smoothed but tip region diverges and curls.

Numerical results that indicate the conformity of the actual shape to the desired shape are shown in Fig 8.3a & 8.3b which compares normalized least squares displacements *LSw*, slopes *LSSx, LSSy* and curvatures *LSKxx, LSKyy, LSKxy*, as defined in Eq. (7.2), (8.4), (8.10). Note that these 6 quantities are normalized further with respect to their counterparts in Case 1 - which uses the displacement criterion only. Fig. 8.3b is the magnified version of Fig 8.3a, excluding the *LSw* values which are usually much larger than 1. The following observations are made from Fig 8.2 and Fig. 8.3:

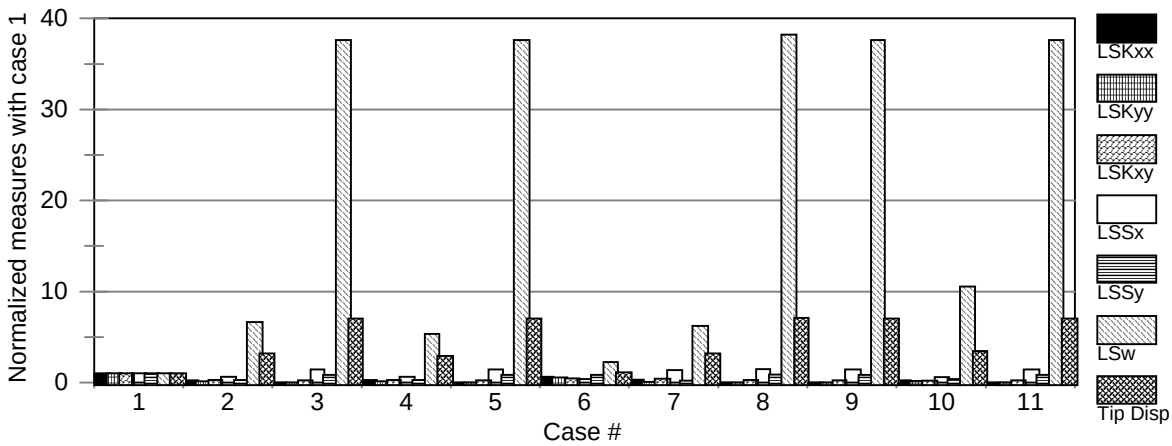

Figure 8.3a. Least square measures of displacement *LSw*, slopes *LSSx, LSSy* and curvatures *LSKxx, LSKyy, LSKxy* and tip displacement at free corner for MCSC using McLLS.

1. The inclusion of any other criteria besides displacements, increases the differences in displacements between the desired and actual shape, i.e. *Lsw(case i) / Lsw(case 1) > 1*, where *i=2...11*. Graphically, this can be seen in Fig. 8.2a as the case that uses the displacement criterion only (case 1), having the best match between actual and desired shape among the other cases, although the structure appears bumpy.

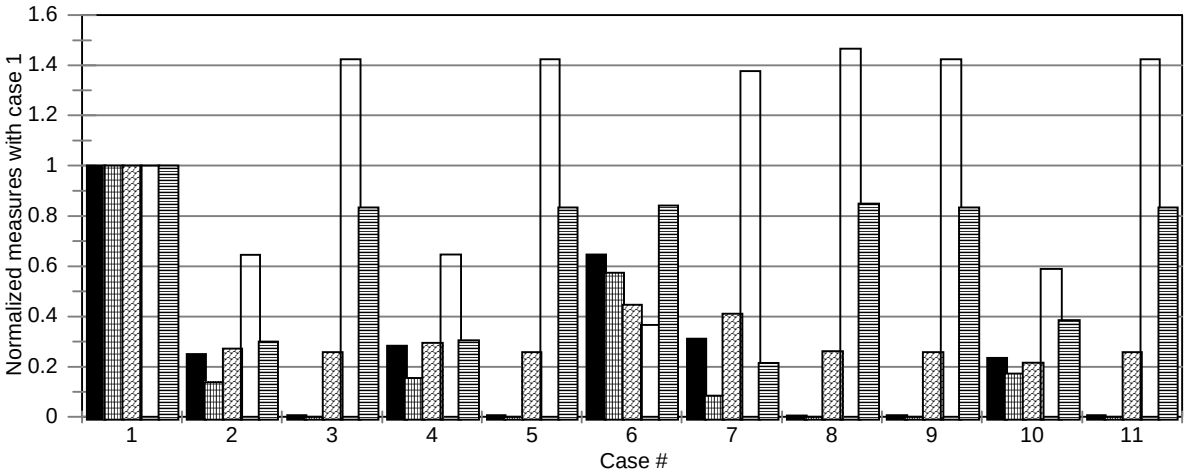

Figure 8.3b. Magnified version of Fig 8.3a - excluding *LSw* and tip displacement.

2. In terms of matching displacements, graphically (Figs 8.2) the 11 cases fall into 6 distinguishable groups. This is reflected in Fig. 8.3a where the *LSw* values for the 11 cases fall into 6 distinct ranges.
3. Cases 3, 5, 8, 9, 11, (see Fig 8.2c) show the worst match for displacements, i.e. highest *LSw* values and the greatest divergence in displacement at either of the free corners. The common feature here is the use of either the K_{xx} or the K_{yy} as the SC criteria. This infers the dominance of these two curvature criteria, meaning that if they are used as control criteria, then all other criteria has almost no influence. Thus the algorithm forces the structure to conform to the desired curvatures strongly while neglecting the other criteria. Not surprisingly for these 5 cases, there is drastic reduction in the *LSKxx* and the *LSKyy* values with respect to case 1, see Fig 8.3b. The slopes S_x did not perform that well either.
4. The similarity between results from case 2 and 4 indicates that both slopes S_x and S_y criteria dominate over the displacements. Case 10 is also quite similar to cases 2 and 4 in terms of reducing the overall LS values. Case 10 which controls the K_{xy} does show some curving effects near the tips as shown in Fig.8.2f.
5. The S_y slope seems to dominate slightly over S_x because comparing cases 2, 4, 6, 7, the exclusion of the S_x criteria in case 7 still produced quite similar results to cases 2 &4. The slope criteria S_y also reduces the curvature measures *LSKxx, LSKyy, LSKxy* quite significantly, even though none of the curvature criteria are used. On the other hand when S_y is excluded in case 6, the dominant criteria is S_x and this criteria seems to be the best at improving the slope measure *LSSx* as well as the displacement measure *LSw*. Hence Fig 8.2d is the one with the second best match in displacement next to case 1 which is

purely displacement controlled.

To recapitulate the observations, slopes and curvatures tend to dominate over the displacement criteria, such that the presence of slope or curvature criteria means it is difficult to control displacements. When the curvatures or slopes are improved (less bumpiness and lower *LS* values for slopes and curvatures) then the displacements, especially at the tip of the cantilever, diverges from the desired shape even more. However, the focus on improving the slopes, especially S_y, also result in significant improvement in curvature without having to control curvature directly.

The set of observations above is based on inducing this *Grid* model (Fig. 8.1) to conform to the desired twist shape of Eq. (7.18). Thus the observations does not necessarily apply to all shape control problems. A few points that can be generalized are: i) Some criteria may have strong dominance over the others. ii) The displacement criteria may be weak, therefore while other criteria are controlled, the resultant displacements may not conform satisfactorily to the desired shape. iii) It is difficult if not impossible to improve all criteria simultaneously for all shape control problems. As a further note, the method of Simulated Annealing (SA) has also been used to conduct MCSC, however the results did not reveal anything extra over the observations made by McLLS. Most of the SA results indicate similar drawbacks to the McLLS method and so it is not necessary to present their results here.

In this simple series of eleven tests, the weights are only given the values of 0 or 1 which means their corresponding criteria can either be switched on or off. In reality, there is an infinite combination of weights that are possible. Even in this series of 11 tests, there is a large amount of information relating to the significance of the criteria and yet there is no clear result as to which case gives the best final result. In fact there is no best result and some cases produce better conformity to the desired shape in certain criteria than others. Thus, what is needed is an algorithm that automatically reduces the bumpiness by improving the slope or curvature criteria and yet not allowing the displacement criteria to deteriorate beyond a given level - this is the objective of the algorithm developed in the next section, known as the Perturbation Buildup Voltage Distribution.

8.5 Perturbation Buildup Voltage Distribution algorithm for SDSC

8.5.1 Introduction to PBVD

The previous section has shown that it is possible for MCSC to "smooth" the bumpiness

of the transverse displacements to the extent that some curvature measures such as *LSKxx* and *LSKyy* are almost zero in comparison to using only the displacement criterion, (case 3 in Fig. 8.3b). Graphically, in Fig 8.2b and Fig. 8.2c for instance, the central part has been smoothed considerably, but the edges have diverged from the desired shape. It appears that the displacement measure, *LSw*, and the slope and curvature measures are conflicting criteria. Improving some criteria can sometimes worsen the other criteria. Due to this reciprocal relationship, the use of McLLS for MCSC is not very efficient because the optimization problem would be dependent on the weights of each criteria. It is quite difficult to select appropriate values for the weights that will reflect the desired importance of each criteria. In addition, the dominance of certain criteria must be neutralized somehow before all the criteria can be compared impartially. Neither of this can be done systematically in McLLS. The use of McLLS would then become a manual process where the user must conduct an initial parametric study on the weights.

To overcome the difficulties with the McLLS method, a new algorithm, called the Perturbation Build Up Voltage Distribution (PBVD) is developed here. Unlike McLLS, PBVD does not require the system to be linear, hence it can be used for general non-linear piezo-elastic systems. However, for linear systems such as the present one, the use of linearity will greatly improve the computational efficiency of the algorithm. The main advantage of this algorithm is that it allows the user greater control over the optimization procedure because it was developed specifically for shape control. The PBVD in this section is developed for two types of criteria, viz the displacement and the slopes. Hence the current PBVD is for SDSC only since this is the first development of PBVD. The basic concept is to minimize the difference in displacements and then to iteratively perturb the system in an effort to minimize the slope difference as well. Slope has been chosen because it was shown in §8.4 that improving the slope difference will also improve the curvature difference between the actual and the desired shapes, thereby reducing the bumpiness of the structure.

PBVD is an iterative - heuristic technique and the concept is to build up voltages on the patches that are significant in changing the structure to the desired shape according to the slope and displacements. It implicitly targets regions that need the most improvement by iteratively correcting the slopes locally to conform to the desired shape. A consequence of PBVD will be the smoothing of the actual structure because the slope is being controlled. And this is achieved without significant sacrifice of the target displacement. Although the name and concept of the algorithm is derived by BVD (a purely displacement based shape control, see Chap. 7) the PBVD

algorithm is significantly different.

8.5.2 The PBVD algorithm for SDSC

The PBVD method starts with the initial configuration which is the resultant of pure displacement based shape control (DBSC) using LLS. The strategy involves improving the slope of the structure on an elemental basis - where the elements with larger slope discrepancies (compared to the desired slope values) will be improved first. The voltage required to improve the slope in an element will be calculated such that only small improvements are made at each iteration, hence requiring only small amounts of incremental voltage at a time. Since PBVD involves perturbing a displacement optimized configuration, unlike BVD which starts from an unknown configuration, there will be no voltage scaling here.

8.5.2.1 Displacement and Slope Measures

The measure of transverse displacements is the *sum of the squared difference* Δw, (Eq. (8.16)) between the desired and the actual nodal values of the entire structure. Note that *LSw* is the normalized counterpart of Δw. There is no need to normalize the displacement and slope measures because they are not optimized simultaneously as before. The slopes are measured on an elemental basis hence the *area integral of the squared difference* (ΔSx^e, ΔSy^e) between the desired and actual slope is used. This has the advantage of placing more importance on the improvement of slopes of larger sized (area) elements. The new slope-area measures, are defined in Eq. (8.17) and are different from *LSSx*, *LSSy* (Eq. (8.4)) which are the sum of slopes at specific points of the whole structure.

$$\Delta w = \sum_{i=1}^{N_n} (w_i - w_i^d)^2 \tag{8.16}$$

$$\Delta Sx^e = \int_{Ae} (S_x^e - S_x^{e\,d})^2 dA_e \quad ; \qquad \Delta Sy^e = \int_{Ae} (S_y^e - S_y^{e\,d})^2 dA_e \tag{8.17}$$

8.5.2.2 Displacement - Slope Dual Criteria

To investigate the voltage perturbation effect on the slope, the slope of the current iteration is compared with the slope of the previous iteration with respect to the desired slope. Since the displacement and slope criteria may compete with each other, the improvement of the slope of the structure will be at the expense of achieving the desired displacement. By incorporating a tolerance factor *p*, it is possible to aim for an improvement in the slope while restricting the displacement criteria from deteriorating excessively. This dual criteria is expressed

in Eq. (8.18).

$$\begin{aligned}
\int_{Ae}(S_x^{\,e}-S_x^{\,e\ d})^2 dA_e &< (1-p)\int_{Ae}(S_x^{\,e\ o}-S_x^{\,e\ d})^2 dA_e \\
\int_{Ae}(S_y^{\,e}-S_y^{\,e\ d})^2 dA_e &< (1-p)\int_{Ae}(S_y^{\,e\ o}-S_y^{\,e\ d})^2 dA_e \\
\sum_{i=1}^{N_n}(w_i-w_i^{\,d})^2 &< (1+p)\sum_{i=1}^{N_n}(w_i^{\,o}-w_i^{\,d})^2
\end{aligned} \tag{8.18}$$

where superscript d = desired quantities and o = previous iteration quantities.

During each iteration, an incremental voltage dV will be added temporarily and the effects on the slope of the other elements as well as displacements are checked. If the side effects of adding dV are tolerable, then it is added permanently and the new voltage configuration will be used as the base configuration in the next iteration.

Since the mathematical model is linear, PBVD can be made more efficient by using the linearity of displacements and slopes with respect to voltages This step will be skipped when applying PBVD to non-linear models. By using the linear influence coefficients as shown in Eq. (7.1) & (8.3), when the voltage is perturbed at the kth patch only, the dual criteria in Eq. (8.18) is re-expressed as Eq. (8.19) and enable the calculation of the optimum incremental voltage dV. Only one of the slope equations in Eq. (8.19) is solved simultaneously with the displacement equation, depending on which slope needs more improvement. So two parabolic equations are solved simultaneously using a method called Dual Quadratic Minimization (DQM), developed here to find the minimum point in the intersection region of two upright parabolas. The solution dV represents the incremental voltage used for perturbing the kth patch.

$$\begin{aligned}
p\int_{Ae}(S_x^{e'})^2 dA + 2dV\int_{Ae}(S_x^{e'})(C^{Sx\ e})_k dA + dV^2\int_{Ae}(C^{Sx\ e})_k^2 dA &< 0 \\
p\int_{Ae}(S_y^{e'})^2 dA + 2dV\int_{Ae}(S_y^{e'})(C^{Sy\ e})_k dA + dV^2\int_{Ae}(C^{Sy\ e})_k^2 dA &< 0 \\
-p\sum_{i=1}^{N_n}(w_i')^2 + 2dV\sum_{i=1}^{N_n} w_i' C_{ik}^{\,w} + dV^2\sum_{i=1}^{N_n}(C_{ik}^{\,w})^2 &< 0
\end{aligned} \tag{8.19}$$

$$\text{where } S_x^{e'} = S_x^{e\ o} - S_x^{e\ d}\ ; \quad S_y^{e'} = S_y^{e\ o} - S_y^{e\ d}\ ; \quad w' = w^{\,o} + w^{\,d}$$

8.5.2.3 Slope Patch Insensitivity

Another quantity that is required in PBVD is the Slope Patch Insensitivity index (SPI^{Sx}, SPI^{Sy}). The SPI^{Sx} is defined in Eq. (8.20) and SPI^{Sy} is defined similarly, although not shown. It

is defined as the ratio of a unit change in voltage to a change in the slope measure between the current (trial) and the previous (base) configurations. Large *SPI(k,e)* values implies that element *e* is insensitive to the voltage applied to patch *k*.

$$
\begin{aligned}
SPI^{Sx}(k,e) &= \frac{V_k - V_k^o}{\Delta Sx^e - \Delta Sx^{eo}} \\
with \quad V_k &= V_k^o + dV \; ; \quad where \; dV = 1.0 \\
SPI^{Sx}(k,e) &= \frac{1}{\int_{Ae} (C^{Sx\,e})_k ((C^{Sx\,e})_k + 2S_x^{e\,/})\; dA_e}
\end{aligned}
\tag{8.20}
$$

The SPI differs from DPI (Displacement Patch Insensitivity, Eq. (7.15)) in that the former does not need to be normalized because in PBVD, the slopes are optimized separately from the displacements. Note that the *SPI* values also depend on the base configuration, S_x^{eo}, found inside S_x^{e}' in Eq. (8.20).

The DPI in Chap. 7 was used as an indicator or tool that assist location optimization in DBSC but it was not used directly in the BVD algorithm. Since BVD optimizes the shape by using the displacements only, and the fact that the displacement is linear with respect to voltage, makes it a scalable problem. On the other hand since PBVD perturbs the system from a base configuration, the displacements, slopes and voltages are not directly scalable. Therefore the SPI has been quite useful in the PBVD algorithm in determining which are the best patches to perturb at each iteration in order to correct the slope of a certain element.

8.5.2.4 PBVD Pseudocode

The PBVD algorithm is summarized as follows:

1. Perform pure displacement shape control using LLS and use the resultant voltage configuration as the initial configuration for PBVD.
2. Calculate Δw and (ΔSx^e), (ΔSy^e) for all elements *e*.
3. Sort the (ΔSx^e), (ΔSy^e) from the highest magnitude to the lowest.
4. Select an element with high (ΔSx^e) or (ΔSy^e) to be improved upon. A normal probability distribution selection mechanism is used so that elements with higher (but not necessarily the highest) (ΔS^e) magnitude are more likely to be selected.
5. Calculate $SPI^{Sx}(k,e)$ and $SPI^{Sy}(k,e)$ for the kth patch and the eth element for all patches and all elements.
6. Sort the slope sensitivities among all patches, for the selected element.

7. Begin iteration of voltage perturbation starting from the most sensitive patch.

8. Calculate incremental voltage dV necessary to improve slope for this element but with a tolerable worsening in displacement (using tolerance factor p). This is done by finding the optimum dV of Eq. (8.19).

9. Apply dV and recalculate Δw for the structure and (ΔSx^e), (ΔSy^e) for all elements.

10. Check for adverse effects in the slopes of other elements when dV was applied to patch k. If the slope of the other elements are within a tolerable limit (indicated by tolerance factor s) then accept the new voltage configuration and begin the next iteration in step 2. Otherwise, go to step 7 to perturb the next patch.

11. Continue iteration until maximum number of iterations is reached or total tolerance (LSd) on original displacement measure Δw is exceeded.

There are several ways in which PBVD has provided a more intuitive control mechanism over generic optimization routines. For example the total tolerance LSd in step 11 specifies the limit below which the worsening of the displacement measure is tolerable. During the iteration, the voltages are calculated such that there is a small improvement in the slope of the element and at the same time the displacement measure must not worsen by a certain amount. In general, the PBVD technique implicitly targets region whose slope needs the most improvement. Unlike the McLLS method, there is no need to determine the appropriate weights of each criteria - the user only need to specify the desired amount of improvement and the tolerances of displacements. The flowchart of PBVD algorithm is shown in Appendix H.

8.6 Performance of PBVD in SDSC

Investigations in §7.5 has shown that using the LLS method to achieve pure displacement SC may have matched the nodal displacements well, but the LLS method contain no mechanism that monitors the slope of the structure. Hence the overall twisting effect was achieved but there are regions of bumpiness (see Fig 8.2a). In the next stage, the slopes and curvatures were incorporated into the McLLS method and this simultaneous MCSC shows significant improvement at the center of the structure which has been smoothed. However, the tip displacements worsened. Improvements could be made by making use of weights but therein lies the disadvantage of having to choose the weights arbitrarily.

PBVD is a less rigid alternative to McLLS; it incorporates an element of randomness in the iterative process and does not require weights. Instead it allows the user more direct control

by specifying various tolerances in the iterative algorithm. The same test from §8.4 is repeated here using PBVD for SDSC. Table 8.2 lists the different parameters for the example cases presented in this section and their corresponding results are in Fig. 8.4. The parameters of PBVD are the tolerance mechanisms such as *LSd* - the displacement tolerance above which the PBVD iteration will discontinue, *Mult.Iter* - a multiplication factor that determines the maximum number of iterations above which the PBVD will also discontinue, *p* - the *p* factor of Eq. (8.18) that determines the incremental improvement in slope and the tolerance in displacement for each iteration, *s tolerance* - the tolerance allowed for the slopes of other elements when the slope of a specific element is improved at each iteration. In Table 8.2, the iterations of the first two cases were automatically stopped as it exceeded the *LSd*. The *s* and *p* tolerances influences the speed and the amount of improvement made - a large value would signify a coarse iterative approach which may not yield good solutions. From numerous other tests, favorable results seemed to be obtained when *p* and *s* are of the orders of magnitude of *0.01* and *1* respectively.

Table 8.2. Parameters for several case of SDSC using PBVD.

Parameters\Case	1 (ref.)	2	3	4	5	6 (McLLS)
LSd Tolerance	-----	0.05	0.5	5.5	5.5	-----
Mult. Iter	-----	1.9	1.9	100.9	100.9	-----
p tolerance	-----	0.001	0.01	0.01	0.1	-----
s tolerance	-----	0.3	0.3	2.3	30.03	-----

Cases 2-5 in Fig. 8.4 shows the changes in the *least square* measures for displacements, slopes and curvatures using PBVD for SDSC. The reference case 1 is the case using displacement based shape control (DBSC). Since the other cases are normalized with respect to their corresponding criteria in case 1, the results of Fig. 8.4 indicate the level of improvement for each criteria when PBVD is used in comparison with using LLS in DBSC. For this particular example, it was the slope in the y-direction that required more improvement. This was automatically determined by the PBVD algorithm and all PBVD cases in Fig. 8.4 shows the reduction in *LSSy*, hence improvement on the slope in the *y*-direction was achieved. From other data not published here, the slope in the *x*-direction in general was an order of magnitude better than its counterpart and thus does not have a high priority for improvement. Fig 8.4 also shows that as *slope y* improves, *slope x* slightly worsens but in absolute terms, the slope in the *x*-direction is still better.

Due to the conflicting nature of displacement and slope, when the slope in the y direction improves, the displacement deteriorates as shown in Fig 8.4. In the case 2 when slope was improved by 8%, the displacement worsened by 5% and in the case 5 when the slope was almost

improved by 50%, the displacement deteriorated by 176%. Note these values are cumulative over the 339 nodal points hence the value for each point is in fact much lower. Hence it depends on the specific application as to how much improvement in the slope is required and how much deterioration in the displacement criteria is tolerable.

Comparing the present set of PBVD results (Fig. 8.4) with the results using McLLS in §8.4 (Fig. 8.3a & Fig. 8.3b), the most obvious difference is the improvement in the ability to maintain displacement conformity between the *desired* and *actual* shape. Using McLLS (Fig 8.3a) it is very easy for the displacement of the actual shape to diverge from the desired shape, for example the *LSw* can be up to 40 times the case of using pure displacement control. Using PBVD the displacement tolerance mechanism is built into the algorithm and cases 2-5 constraints *LSw* to be less than 1.05, 1.5, 6.5 and 6.5 times the *LSw* for pure displacement control respectively. Cases 4 & 5 have converged with *LSw* approximately 1.9 & 2.8 without needing to reach the allowed value which is 6.5 for both. Also note that in McLLS, the tip displacements are usually much lower than the *LSw* values whereas the results from PBVD produces tip displacements similar to *LSw* values. This indicates that in McLLS, the resultant shape may be quite different from the desired shape across the whole plane of the structure, whereas in PBVD, there is much better conformity throughout the plane of the structure - compare Fig. 8.5 with Fig. 8.2c.

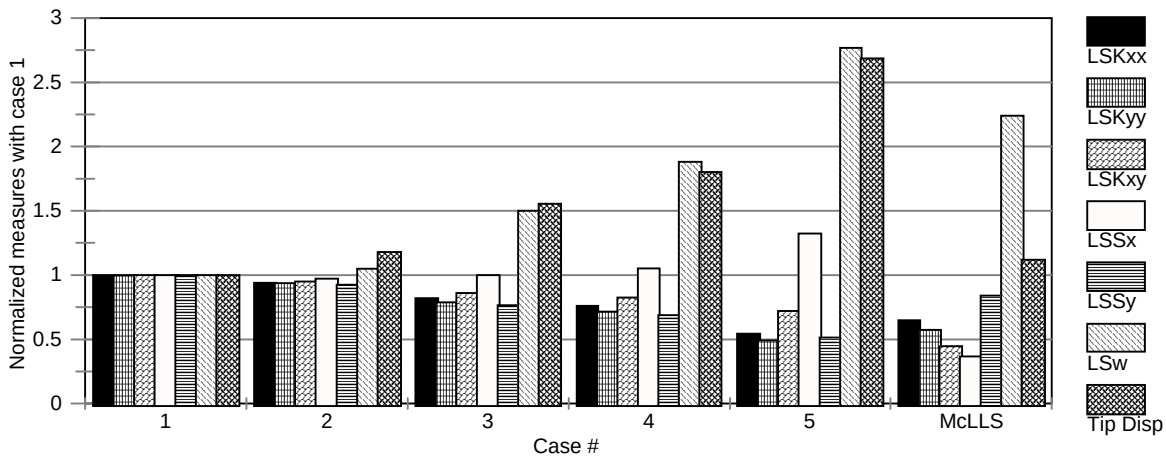

Figure 8.4. Least square measures of displacement *LSw*, slopes *LSSx, LSSy* and curvatures *LSKxx, LSKyy, LSKxy* and tip displacement at free corner for SDSC using PBVD.

The last case displayed in Fig 8.4 correspond to case 6 of §8.4 - it is among the best out of the 11 cases using McLLS. When applying the McLLS or any other generic optimization algorithms on MCSC, it is very difficult to obtain a desirable result without much trial and error in varying the weights of each control criteria. On the other hand, equivalence performance can

be achieved by PBVD with much less effort because it is a method that can be used methodically to obtain the desired configuration by specifying the appropriate tolerances. The 3D view of the transverse displacement *w* at the mid-plane for case 5 is shown in Fig. 8.5. Comparing with Fig. 8.2a which used the displacement criteria only, in Fig 8.5 the regions at the edges of the cantilever plate where there was most bumpiness, have been smoothed. This improvement comes at the expense of the displacement criteria where the tip displacement is noticeably increased.

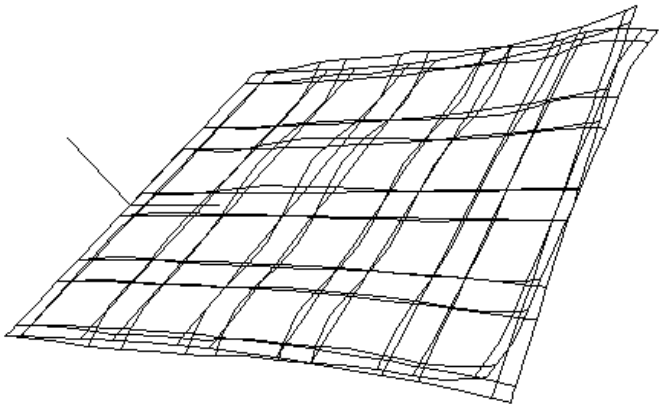

Figure 8.5. Cantilever plate after PBVD-SDSC procedure, case 5. Oblique full field view of the transverse displacement.

The two figures Figs. 8.6a & 8.6b show the improvement in the slope and curvature respectively across a sample cross section of the structure. Specifically, Fig. 8.6a is the normalized slope measure ΔSy^e as defined in Eq. (8.17), plotted along the *x*-direction at $y=-4.5x10^{-2}m$ for the first 5 cases of Table 8.2. Essentially ΔSy^e measures the difference between the slope S_y of the actual shape and the desired shape. Clearly case 5 shows the greatest improvement comparing to the reference case 1.This is expected because PBVD has chosen to improve S_y in regions which needs the most improvement. An unforseen result of PBVD in this case is the improvement in the curvature K_{yy} too, as indicated by the graph of the curvature measure (defined later) shown in Fig 8.6b. The intrinsic relationship between the slope and curvature in the *y*-direction is also indicated by the similarity in shape of both graphs.

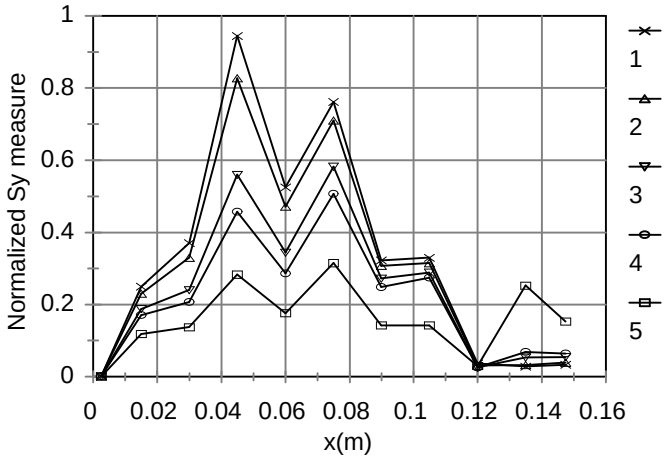

Figure 8.6a. Normalized slope measure for S_y for each element for 4 PBVD-SDSC cases and a reference case.

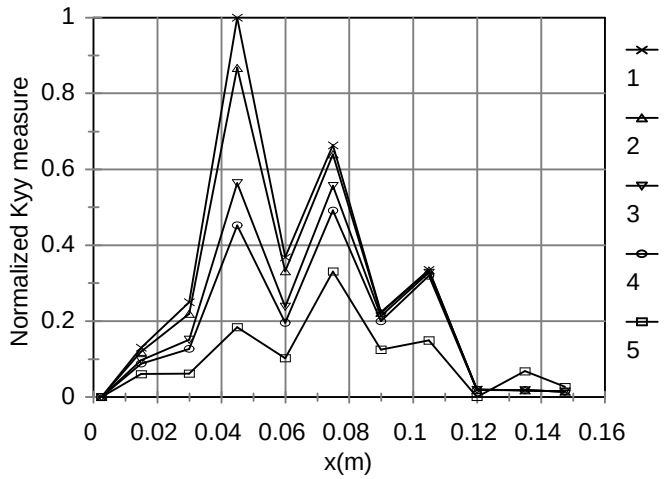

Figure 8.6b. Normalized curvature measure for K_{yy} for each element for 4 PBVD-SDSC cases and a reference case.

8.7 Stress Reduction Effects due to SDSC using PBVD

The existence of complex stress fields within a smart structure should be expected because of the independent localized actuators distributed throughout the structure. The greater number of independent active patches, the greater is the shape controllability. This is analogous to providing the structure with enough actuation degrees of freedom in order to achieve a complex shape which can be thought of as a combination of basic shapes. By imposing voltages on the actuators, the structure is being coerced into the desired shape. This effect is more forceful in the LLS method because it is a direct approach whereas the iterative approach of PBVD is more relaxed in its process of calculating the voltage distribution. In either case, when significantly different voltages are applied to various patches, as directed by the shape control algorithm, localized internal stresses are set-up. This issue is particularly significant to smart

structures since the actuators are not external but are regarded as an integral part of the structure. Note that the increase in shear stress around the edges of a square PZT region was also observed by Batra & Liang (1996).

The bumpiness of the shape of the structure are in fact changes in slope in localized regions. This means the local curvature has a higher than usual magnitude. In practical terms, this translates to high stresses in certain regions as well as large variation in stresses between other regions. Since the PBVD algorithm has the ability to smoothen the structure, it can be regarded as a secondary procedure in shape control to reduce internal structural stress caused by the primary stage which is pure displacement shape control. This conjecture will be validated by the results obtained using the PBVD algorithm .

The following results compares the internal stresses generated within the structure as a result of the pure displacement shape control using LLS and the stresses obtained after the PBVD procedure is applied. The test model is the same as that in §8.4 and for the PBVD case, the set of parameters corresponding to case 5 from Table 8.2 (§8.6) was used. The stresses for each element are calculated at their 2x2 Gauss points at a height of $z=9.0x10^{-4}m$, which is within the Aluminum substrate. Although all six stresses were calculated, only a selection of the results are presented here due to space limitation. The normal in-plane stresses at $y=-3.923x10^{-2}m$ along the length of the structure is shown in Fig. 8.7a - dashed lines for stresses without PBVD and solid lines for stresses with PBVD. There is a clear reduction in the σ_{yy} stress along the entire length of the structure and it is mainly tensile stresses. Several points with high σ_{xx} stress magnitudes were also reduced significantly and also note that this stress is compressive in some regions and tensile in others.

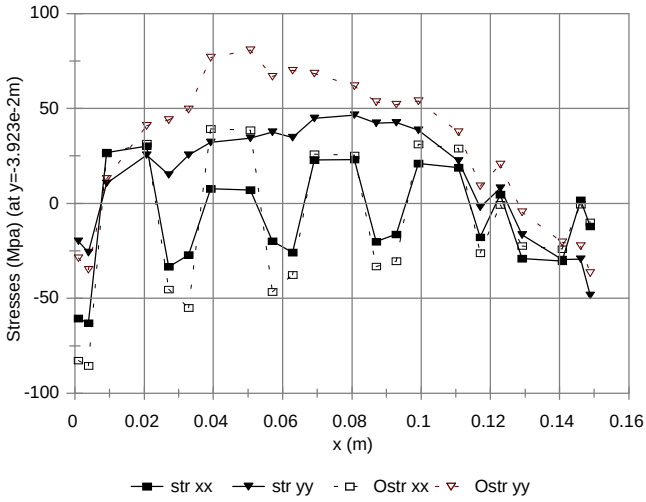

Figure 8.7a. Reduction of the normal in-plane stresses by the PBVD-SDSC procedure (y-section).

The in-plane shear stress (τ_{xy}) and one of the transverse shear stresses (τ_{yz}) are plotted in Fig. 8.7b at $y=-3.923x10^{-2}m$. Although the transverse shear stress may be smaller in magnitude compared to the other stresses, it is clearly not negligible. This justifies the need to use a displacement field such as the TODL formulation that is able to capture the transverse shear effects. From Fig. 8.7b it can be seen that at points with high stress magnitudes, applying PBVD would reduce their magnitudes significantly. This effect is consistent with the PBVD algorithm which was founded on the premise of reducing the worst local effects.

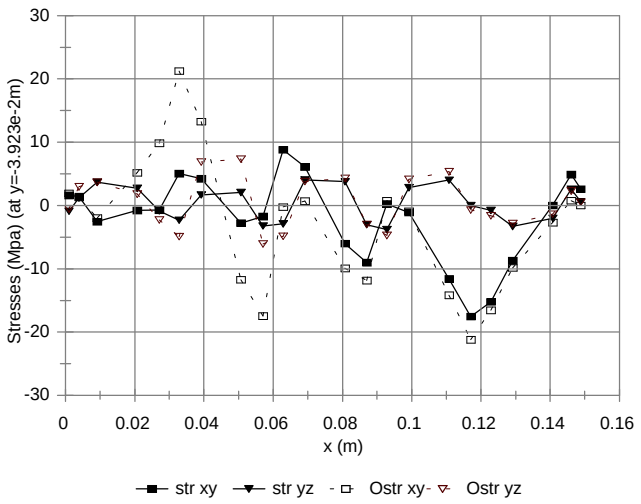

Figure 8.7b. Reduction of a transverse and in-plane shear stress by the PBVD-SDSC procedure (y-section).

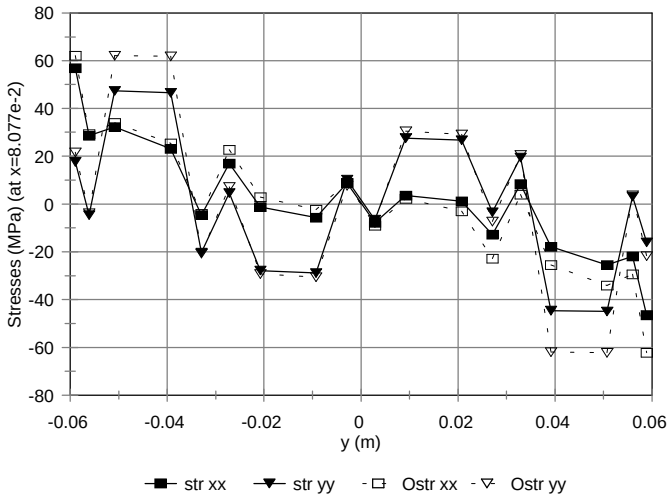

Figure 8.7c. Reduction of the normal in-plane stresses by the PBVD-SDSC procedure (x-section).

The normal in-plane stresses at the perpendicular cross-section, $x = 8.077x10^{-2}m$, are plotted in Fig. 8.7c while the transverse and in-plane shear stresses are found in Fig. 8.7d. This cross-section is almost at the center of the cantilever plate running across its width. Regions of

high stresses in both Figs. 8.7c & 8.7d has been significantly reduced. For example in Fig.8.7c, the maximum reduction of σ_{yy} of approximately 60MPa to 45MPa (25%) was achieved, while in Fig. 8.7d the in-plane shear (twist) stress τ_{xy} was reduced from 18MPa to 11MPa (38%) at one region.

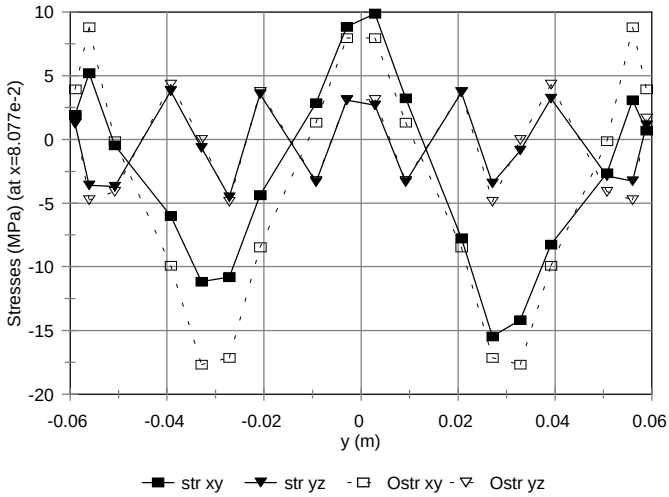

Figure 8.7d. Reduction of a transverse and in-plane shear stress by the PBVD-SDSC procedure (x-section).

Note that in all graphs, the zig-zaggedness of the stress distribution is quite evident and this is a reflection of the discrete actuator patch layout of the physical structure. Thus these discrete effects due to the presence of the patch actuators are quite significant, as shown by the results, and should not be ignored in real practical applications. Also notice that the dotted lines in Figs. 8.7d are symmetrical because the use of LLS for DBSC is able to capture the symmetrical behavior of the in plane shear stress that resulted from the mathematically defined desired shape. However, PBVD is an iterative algorithm and no symmetric constraint has been imposed because it was found that symmetry constraints may hinder the perturbation process thus producing shape measures which are slightly worse off.

8.8 PBVD for Curvature Displacement Shape Control (CDSC)

The goal at the beginning of this chapter is to introduce additional control criteria besides transverse displacements in order to reduce secondary effects in shape control such as the resultant bumpiness of the structure. The development of the PBVD method in §8.5 uses displacement as the base criterion and both of the slopes as the perturbing criteria. This concept is now extended to incorporate curvatures. However, this will remain a dual-criteria curvature displacement shape control (CDSC) where the base criteria is displacement and the perturbing criteria are curvatures instead of slopes. It has been decided not to use slope and curvature

simultaneously as the perturbing criteria since they are two different physical quantities which may have quite different orders of magnitude. Previously, using PBVD for SDSC had also resulted in an improvement in the conformity of the curvatures with the desired shape. Thus in the application of PBVD to CDSC, the conformity of slopes will be observed as well as the effects on the internal stresses of the structure. The PBVD method for CDSC is similar to the PBVD method for SDSC described in §8.5, hence it will not presented in great detail except for several definitions that relate to the curvatures.

8.8.1 Displacement and Curvature Measures

The measure of transverse displacements is the same as that in Eq. (8.16). The curvatures are measured on an elemental basis hence the *area integral of the squared difference* (ΔKxx^e, ΔKyy^e, ΔKxy^e) between the desired and actual curvatures are used. The new curvature-area measures, are defined in Eq. (8.21) and are different from *LSKxx, LSKyy, LSKxy* (Eq. (8.10)) which are the sum of curvatures at specific points of the whole structure.

$$\Delta Kxx^{\,e} = \int_{Ae} (K_{xx}^{e} - K_{xx}^{e\,d})^2 dA_e \quad ; \qquad \Delta Kyy^{\,e} = \int_{Ae} (K_{yy}^{e} - K_{yy}^{e\,d})^2 dA_e$$
$$\Delta Kxy^{\,e} = \int_{Ae} (K_{xy}^{e} - K_{xy}^{e\,d})^2 dA_e \tag{8.21}$$

8.8.2 Displacement - Curvature Dual Criteria

The competing dual criteria, displacement and curvature, are expressed as Eq. (8.22) where the tolerance p is used to specify the improvement in curvature and allowable deterioration in displacement at each iteration. Note that at each iteration, PBVD will choose only one out of the three curvatures, among all elements, which has the worst curvature measure in order to improve upon it.

$$\begin{aligned}
\int_{Ae} (K_{xx}^{e} - K_{xx}^{e\,d})^2 dA_e &< (1-p)\int_{Ae} (K_{xx}^{e\,o} - K_{xx}^{e\,d})^2 dA_e \\
\int_{Ae} (K_{yy}^{e} - K_{yy}^{e\,d})^2 dA_e &< (1-p)\int_{Ae} (K_{yy}^{e\,o} - K_{yy}^{e\,d})^2 dA_e \\
\int_{Ae} (K_{xy}^{e} - K_{xy}^{e\,d})^2 dA_e &< (1-p)\int_{Ae} (K_{xy}^{e\,o} - K_{xy}^{e\,d})^2 dA_e \\
\sum_{i=1}^{N_n} (w_i - w_i^{\,d})^2 &< (1+p)\sum_{i=1}^{N_n} (w_i^{\,o} - w_i^{\,d})^2
\end{aligned} \tag{8.22}$$

where superscript d = desired quantities and o = previous iteration quantities.

The incremental or perturbing voltage dV is implicit in Eq. (8.22) but for a linear

mathematical model, the use of the linear influence coefficients as shown in Eq. (7.1) & (8.9), where the voltage is perturbed at the kth patch only, will enable dV to be expressed explicitly in Eq. (8.23). Solving the displacement and one of the curvature equations simultaneously will determine the optimum incremental voltage necessary to perturb the system.

$$
\begin{aligned}
p\int_{Ae}(K_{xx}^{e'})^2 dA \;+\; 2dV\int_{Ae}(K_{xx}^{e'})(C^{Kxx\ e})_k dA \;+\; dV^2\int_{Ae}(C^{Kxx\ e})_k^2 dA \;&<\; 0\\
p\int_{Ae}(K_{yy}^{e'})^2 dA \;+\; 2dV\int_{Ae}(K_{yy}^{e'})(C^{Kyy\ e})_k dA \;+\; dV^2\int_{Ae}(C^{Kyy\ e})_k^2 dA \;&<\; 0\\
p\int_{Ae}(K_{xy}^{e'})^2 dA \;+\; 2dV\int_{Ae}(K_{xy}^{e'})(C^{Kxy\ e})_k dA \;+\; dV^2\int_{Ae}(C^{Kxy\ e})_k^2 dA \;&<\; 0\\
-p\sum_{i=1}^{N_n}(w_i^{/})^2 \;+\; 2dV\sum_{i=1}^{N_n} w_i^{/} C_{ik}^{w} \;+\; dV^2\sum_{i=1}^{N_n}(C_{ik}^{w})^2 \;&<\; 0
\end{aligned}
\tag{8.23}
$$

$$
where\ \ K^{e'} = K^{e\ o} - K^{e\ d}\ ;\quad w^{/} = w^{o} + w^{d}
$$

8.8.3 Curvature Patch Insensitivity

The counterpart of the SPI is the Curvature Patch Insensitivity (CPI) index. The CPI^{Kxx} which corresponds to the curvature K_{xx} is defined in Eq. (8.24) and CPI^{Kyy} & CPI^{Kxy} are defined similarly, although not shown. CPI has a similar purpose as SPI in the PBVD algorithm, that is to determine which is the best actuator patch (k) to activate to produce the greatest change in element (e).

$$
\begin{aligned}
CPI^{Kxx}(k,e) \;&=\; \frac{V_k \;-\; V_k^{o}}{\Delta Kxx^{e} \;-\; \Delta Kxx^{eo}}\\
with\quad V_k \;&=\; V_k^{o} \;+\; dV\ ;\quad where\ dV \;=\; 1.0\\
CPI^{Kxx}(k,e) &= \frac{1}{\int_{Ae}(C^{Kxx\ e})_k((C^{Kxx\ e})_k + 2K_{xx}^{e'})\ dA_e}
\end{aligned}
\tag{8.24}
$$

The rest of the PBVD algorithm using displacements and curvatures (CDSC) is similar to PBVD for SDSC as described in §8.5 and Appendix H, where reference to slopes are replaced by curvatures, hence will not be repeated here.

8.9 Performance of PBVD in CDSC

A similar set of tests to §8.6 is performed here to illustrate the performance of using curvature as the perturbing criteria. The same structural model and twisted desired shape is used

as in §8.4 and §8.6. The voltage configuration is initialized by first using the LLS method to perform shape control with the displacement criteria only. The resulting voltage configuration is perturbed in order to improve the curvature difference between the desired and the actual shape. A series of tests were conducted where various parameters of the PBVD were varied and a selection of cases representing a wide range of the results is presented here. Table 8.3 shows the main parameters of PBVD while Fig. 8.8 shows the least squares (LS) measures for displacements, slopes and curvatures normalized with case 1 - where only displacement criterion is used in case 1. The LS values measure the differences, of the respective quantities, between the desired shape and the actual shape.

Table 8.3. Parameters for several case of CDSC using PBVD.

Parameters\Case	1 (ref.)	2	3	4	5	6	7	8	9
LSd Tolerance	---	5.5	0.05	0.5	5.5	5.5	5.5	0.5	0.5
Mult. Iter	---	0.5	0.5	0.5	100.9	100.9	1.9	1.9	1.9
p tolerance	---	0.01	0.01	0.01	0.01	0.1	0.001	0.001	0.1
s tolerance	---	2.3	2.3	2.3	2.3	0.01	0.3	0.01	0.0001

It is quite clear from Fig. 8.8 that using PBVD in CDSC has improved the conformity of all three types of curvatures between the desired and the actual shape - i.e. normalized *LSKxx*, *LSKyy* and *LSKxy* values less than 1.0. Hence a quick conclusion is that PBVD has achieved its aim in CDSC by reducing the differences between the curvatures of the desired and actual shape. This in turn has reduced the bumpiness of the structure. However, the problem is more interesting and challenging because tailoring the voltage configuration to minimize curvature difference (or slope difference in SDSC), is at the expense of the conformity of transverse displacements. When there is a good curvature match, the displacement match becomes poorer.

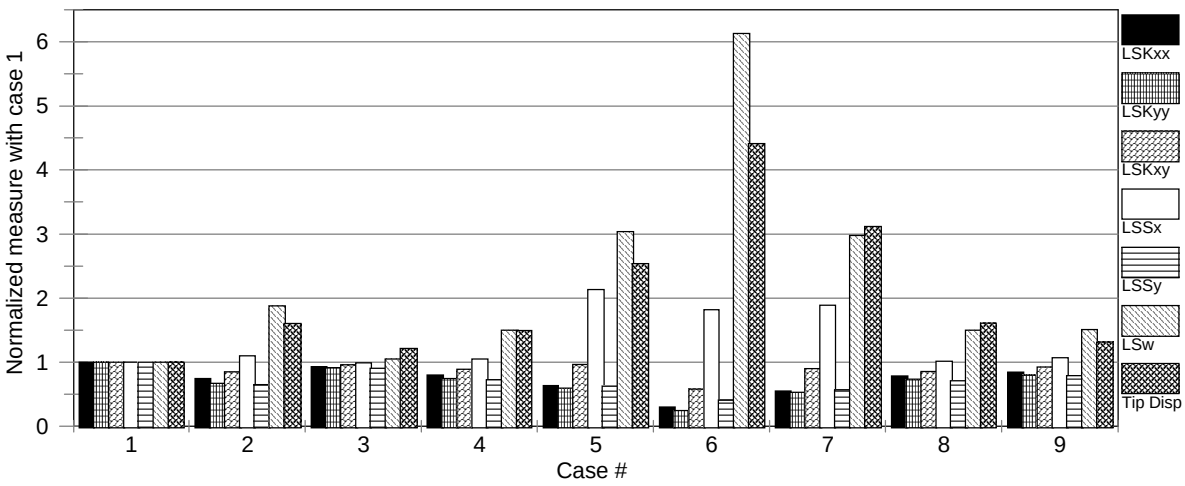

Figure 8.8. Least square measures of displacement *LSw*, slopes *LSSx*, *LSSy* and curvatures *LSKxx*, *LSKyy*, *LSKxy* and tip displacement at free corner for CDSC using PBVD.

Hence a balance is sought between the requirements of a good displacement match and a good curvature match (reducing bumpiness). This is achieved readily by PBVD via parameters such as *LSd* - the tolerance of displacement deterioration or *p* - the tolerance associated with the size of the voltage perturbation. Thus notice in Fig. 8.8 that cases with very low LS curvature values (Cases 5,6,7) also have quite large LS displacement values. In fact case 6 would suitable when there is a strong need to conform to the desired curvatures because *LSKxx, LSKyy, LSKxy* and *LSSy* have improved by *70%, 75%, 40% and 60%* respectively; at the expense of *LSw* and tip displacements increasing by 6 and 4 times respectively. On the other hand cases 2,4,8,9 which have moderately low LS curvature values, have *LSw* values which are not too excessive. Note that for this particular test model, improving the curvatures tend to improve the S_y slope but the S_x slope deteriorates a little.

The parameter *Mult. Iter.* in Table 8.3 is the number of inactive iterations before the algorithm terminates and is similar to a convergence parameter. In cases 5,6,7 where the total displacement tolerance, *LSd*, and *Mult. Iter.* is quite high, it allows the PBVD process to tolerate a greater deterioration of the displacement measure while improving the curvature. In case 2 however, although *LSd* is large, *Mult. Iter.* has a low value, thus the algorithm stops at quite low *LSw* value with good improvement in curvatures obtained. Restricting cases 4,8,9 to have low displacement tolerance *LSd* values, their *LSw* values are never excessively high but yet they can still achieve significant improvement in curvatures. Case 3 has a very strict *LSd* value thus the improvement in curvature is also quite restricted. The tip displacement at one end of the cantilever plate, see Fig. 8.8, is also strongly correlated with the displacement measure *LSw*.

Besides looking at the LS curvature values, the reduction in bumpiness can also be seen graphically. The oblique view of the transverse displacement plots of Case 4 & 7 are shown in Figs. 8.9a and 8.9b respectively. Comparing to the pure displacement control case in Fig. 8.2a much of the region which appear to be uneven or bumpy, especially near the edges, has been reduced in Figs. 8.9a and 8.9b except for the central region. Also note that case 7 (Fig. 8.9b) has a more relaxed displacement tolerance than case 4 (Fig. 8.9a), thus the former is able to improve its curvatures to a greater extent but also notice that its tip displacement has diverged more than the latter.

From the series of tests, it was noted that the *LSd* is one of the important parameters and it determines the extent to which the curvatures can be improved as well as how much the displacement measure is allowed to deteriorate. The other important parameter is the *p* tolerance which controls the degree of perturbation at each iteration. It was found that a low value, for this

case 0.001-0.01, gave reasonable results. A low value of *p* means that perturbation occur slowly with fine steps, whereas high *p* values indicate coarser perturbation steps and may lead to poorer results. Thus the operation of this parameter is quite similar to the *cooling rate* parameter in *Simulated Annealing* which controls the quality of the solution. For this example, *Mult. Iter.* may be taken as *2.0* or above to prevent premature termination of the algorithm while the *s* tolerance, which essentially controls the side-effects of perturbing an element, may be taken as *0.01*. There is a degree of flexibility in choosing the last two parameters within a certain range.

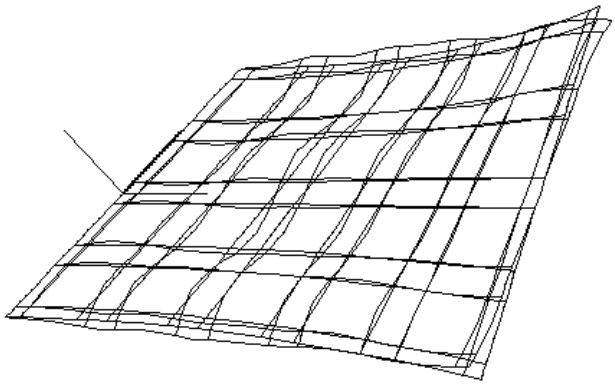

Figure 8.9a. Cantilever plate after PBVD procedure for CDSC, case 4. Oblique full field view of the transverse displacement.

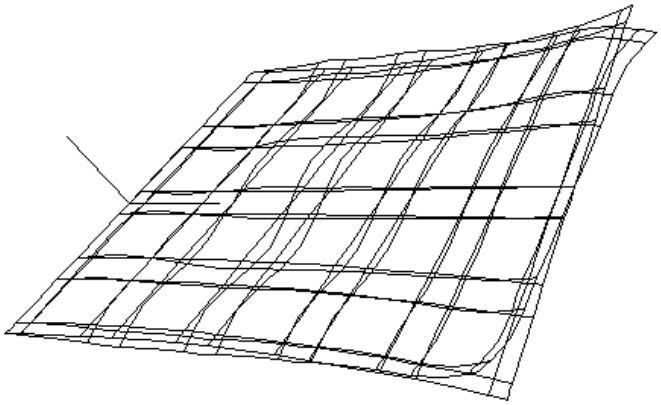

Figure 8.9b. Cantilever plate after PBVD procedure for CDSC, case 7. Oblique full field view of the transverse displacement.

The two figures of Figs. 8.10a & 8.10b can be compared with their counterparts Figs. 8.6a & 8.6b. As before, the normalized curvature and slope measures presented by both graphs are taken along the x-axis at $y=4.5x10^{-2}m$. Cases 7, 8 & 9 are omitted from the graphs because they are quite similar to cases 2, 3 & 5 respectively. The measure for the K_{yy} graph is shown here because among all three curvatures that can be improved by PBVD-CDSC, K_{yy} is the curvature that required the most improvement and therefore the PBVD algorithm automatically focuses

more effort in improving this criteria. One of the positive side-effects illustrated here is that using PBVD to improve the curvature will also result in an improvement of the S_y slope. However, Fig 8.10b shows the conformity of the S_y slope to the desired slope deteriorates considerably near the free end of the cantilever plate for cases 5 & 6. This is not unexpected since cases 5 & 6 were specified to have a higher tolerance of displacement deterioration - this is also reflected in high *LSw* values in Fig. 8.8.

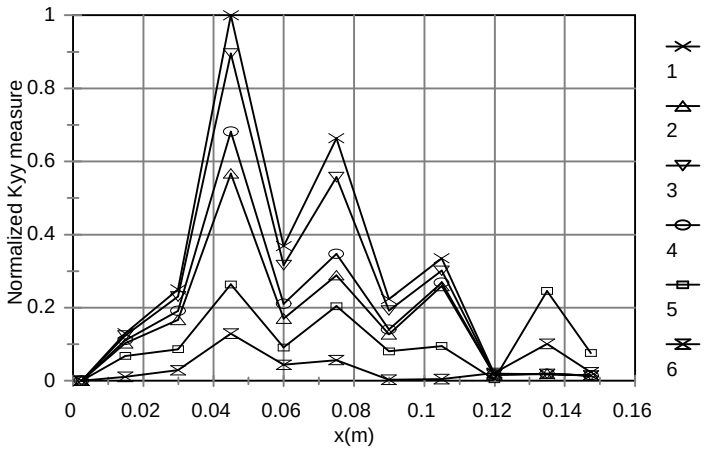

Figure 8.10a. Normalized curvature measure for K_{yy} for 5 cases of PBVD-CDSC and a reference case.

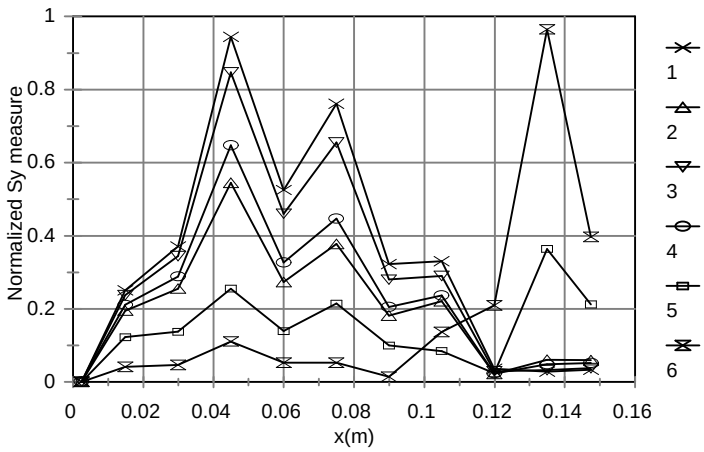

Figure 8.10b. Normalized slope measure for S_y for 5 cases of PBVD-CDSC and a reference case.

The main feature of Figs. 8.10a & 8.10b illustrates that PBVD has achieved reduction in curvature, and in addition the slope S_y, when compared to reference case 1 which uses only displacements for SC. Most cases show that the curvature K_{yy} conforms better (lower values of *LSKyy*) to its desired counterpart. The question as to which of the cases are better depends partly on the user and its application as to the importance of conformity of the curvature versus displacements.

8.10 Stress Reduction Effects due to CDSC using PBVD

The application of the PBVD method in SDSC in §8.7 has shown to cause the reduction of localized stresses in the structure which are attributed to the use of discrete actuator patches. The logical extension of this investigation is to apply PBVD in CDSC in which curvatures are the perturbing criteria instead of the slopes. The results presented here are for the same types of stresses and measured at exactly the same points as the cases in §8.7. The graphs of Figs. 8.11a, 8.11b, 8.11c & 8.11d are the counterparts of Figs. 8.7a, 8.7b, 8.7c & 8.7d.

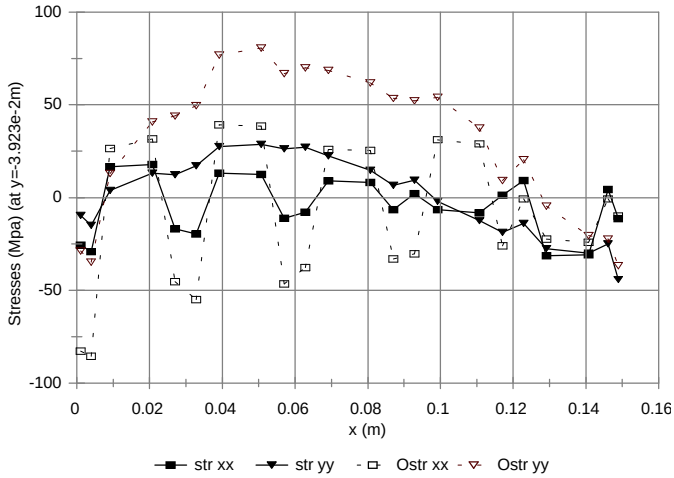

Figure 8.11a. Reduction of the normal in-plane stresses by the PBVD-CSDSC procedure (y-section).

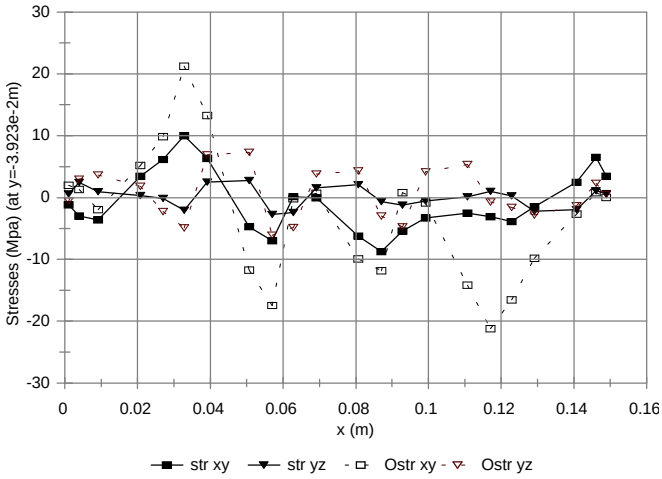

Figure 8.11b. Reduction of a transverse and in-plane shear stress by the PBVD-CDSC procedure (y-section).

The dotted lines in all 4 Figs. 8.11 represent stresses due to using only displacement for shape control. The solid lines correspond to SC using PBVD with curvature criteria. This particular configuration, from which the stresses are measured, correspond to case 6 in §8.9 and it is selected because it produces the most improvement in curvature and slope conformity, see

Fig. 8.8. Hence it is expected to produce significant reduction in stresses. As the 4 graphs of Figs. 8.11 show, there is reduction in the in-plane axial stresses, in-plane shear stresses and transverse shear stresses. Most noticeable are the stress peaks of the shear stresses in Figs. 8.11b & 8.11d, the high axial stress plateau in Fig. 8.11c and the stress profile for σ_{yy} in Fig. 8.11a, all of which are reduced in the CDSC process using the PBVD method. For example in Fig.8.11c, the maximum reduction of σ_{yy} of approximately 60MPa to 16MPa (73%) was achieved, while in Fig. 8.11b the in-plane shear (twist) stress τ_{xy} was reduced from 22Mpa to 5MPa (77%) at one region.

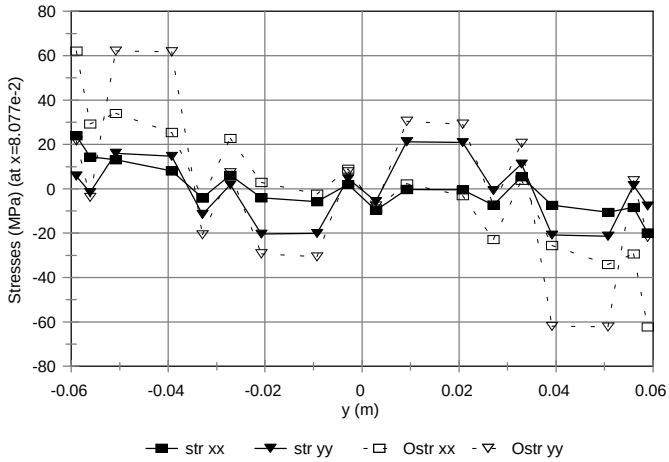

Figure 8.11c. Reduction of the normal in-plane stresses by the PBVD-CDSC procedure (x-section).

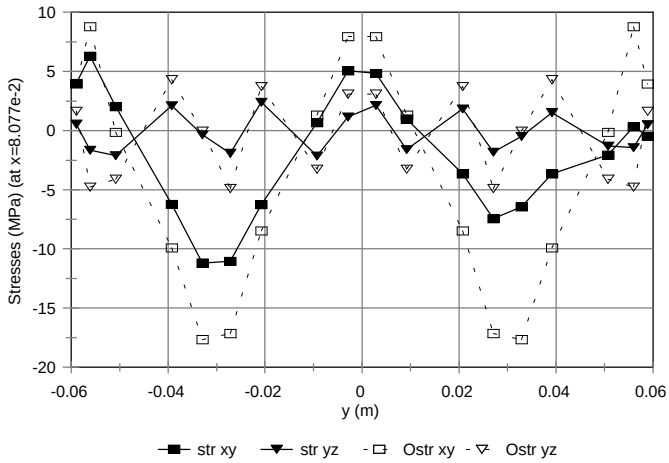

Figure 8.11d. Reduction of a transverse and in-plane shear stress by the PBVD-CDSC procedure (x-section).

Comparison of the stresses obtained by the CDSC process with its counterparts using the SDSC process in §8.7, shows a greater reduction in stresses for the former case. The reason is because CDSC focus on improving the curvature conformity with the desired shape, although the slope conformity does improve alongside, and vice versa for SDSC. Hence as the curvature

criteria improves to a greater extent in CDSC, the stress reduction is also greater since curvature is proportional to stress in classical mechanics.

The graphs of Figs. 8.11 gives an indication of the magnitude of stress reduction at certain cross sections. The discreteness of the actuator patches have considerable effects on the entire stress field as indicated by the abrupt changes in magnitudes over the domain of the structure. The complexity of the stress fields is more readily appreciated by looking at the full field view of the stress field as shown in Figs. 8.12. The 6 pairs of plots in Figs. 8.12 represent the 6 stress components (in Pa), and each pair compare the stresses that results from DBSC using LLS and the additional process of CDSC using PBVD. For all 6 stress components, there are regions in which stresses have reduced quite substantially and there does not appear to be any observable increase in stresses in other regions. In essence, the PBVD for the CDSC process does not only calculate the voltages required to manipulate the structure into a desired shape, it also ensures that its voltage configuration will generate less stresses compared to the case when only the displacement criterion is used.

8.11 Summary

Many existing shape control algorithms are displacement based and they yield reasonable results. From the previous chapter on DBSC, it was observed that better shape controllability requires more independent actuators. However for an extended structure with many independent actuators distributed across the structure, pure displacement based shape control predicts a voltage configuration which when applied, produces regions of bumpiness in the shape due to localized effects. The first attempt to solve this involve MCSC, where slopes and curvatures are incorporated into standard optimization tools in addition to the displacement criterion. Using the McLLS method was only moderately effective because such methods are not flexible. Significant improvement in curvature - slope conformity with respect to the desired shape is usually accompanied by the worsening of the displacement conformity. The generic methods allow limited control over the degree of improvement or deterioration of each criteria.

Hence a dual-criteria shape control algorithm called PBVD was developed firstly using displacement and slope criteria and then another version using displacement and curvature criteria. The PBVD is an iterative algorithm in which the voltages are perturbed and is designed to reduce the bumpiness by targeting some of the worst affected regions using additional slope or curvature criteria. Regions where the desired slope differs most from the actual slope are improved first. Since the displacement and slope are conflicting criteria, the slopes would have

to be improved at the expense of the displacement - the same applies to displacement and curvature. This has been designed into the algorithm to enable the user to decide the extent of the worsening of the displacement criteria that is tolerable. The results have shown that the algorithm is successful in achieving its goal of determining the voltage configuration to actuate the structure to conform to the desired shape and smoothing the structure to a certain extent. The main advantage of PBVD over generic algorithms such as McLLS is that because the former is developed specifically for shape control work, it has an intuitive set of parameters such as displacement tolerance, that allows the user direct control of the MCSC process.

The results are quite dependent on the optimization parameters. The user can have a stricter tolerance on displacement or relax that criteria in order to achieve better improvement in slope or curvature conformity. The two different PBVD algorithms for SDSC and CDSC also provides the choice to focus on either using slope or the curvature as the fine-tuning criteria in shape control. Certainly none of the algorithms, including PBVD, managed to smooth the entire structure as well as conforming perfectly in terms of displacements. But the PBVD method provides a direct means to select a balance between displacement or slope-curvature conformity. For instance, it may be more desirable to have better curvature or slope conformity in a structure for aerodynamic purposes rather than exact displacement conformity to the desired shape.

In addition to smoothing the actual structure's shape, a more practical advantage of this application is that it produces less internal stresses than using DBSC. In real structures where discrete actuators are in operation, although the bumpiness may not always be obvious, the large gradients imply large internal strains and thus large internal stresses. Thus the significance of smoothing extends to alleviating unnecessary internal stresses that could be generated if a purely displacement shape control is used. This prevents over-stressing of the structure and reduce chances of de-bonding in composites applications. Results show that PBVD preferentially reduces the high magnitude stresses to a greater extent than others - especially high stress peaks.

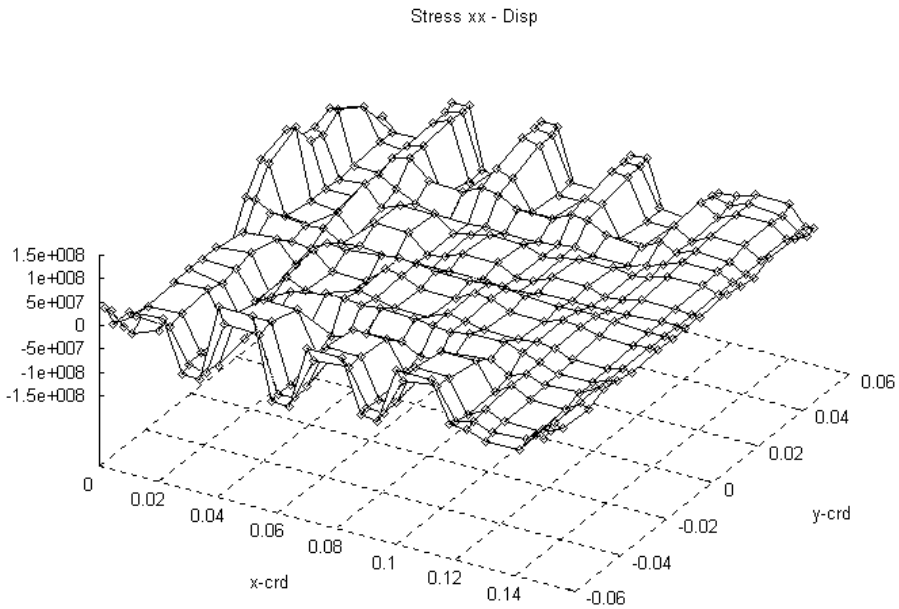

Figure 8.12a. Pure displacement control - Stress xx.

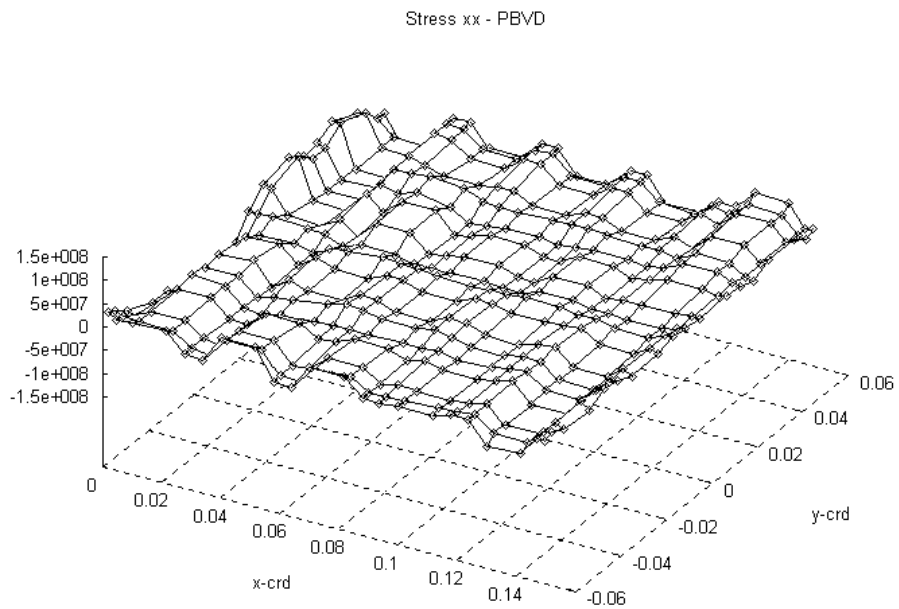

Figure 8.12b. CDSC with PBVD - Stress xx.

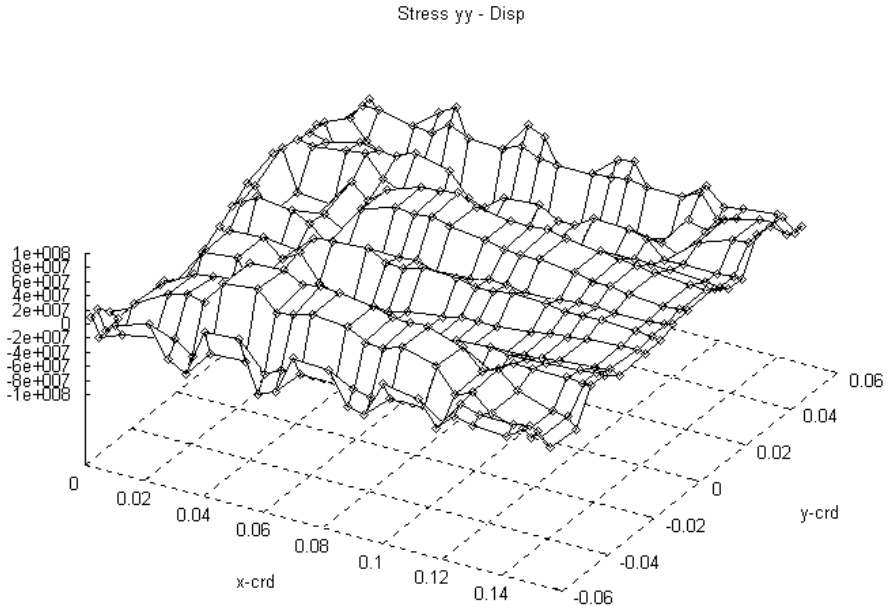

Figure 8.12c. Pure displacement control - Stress yy

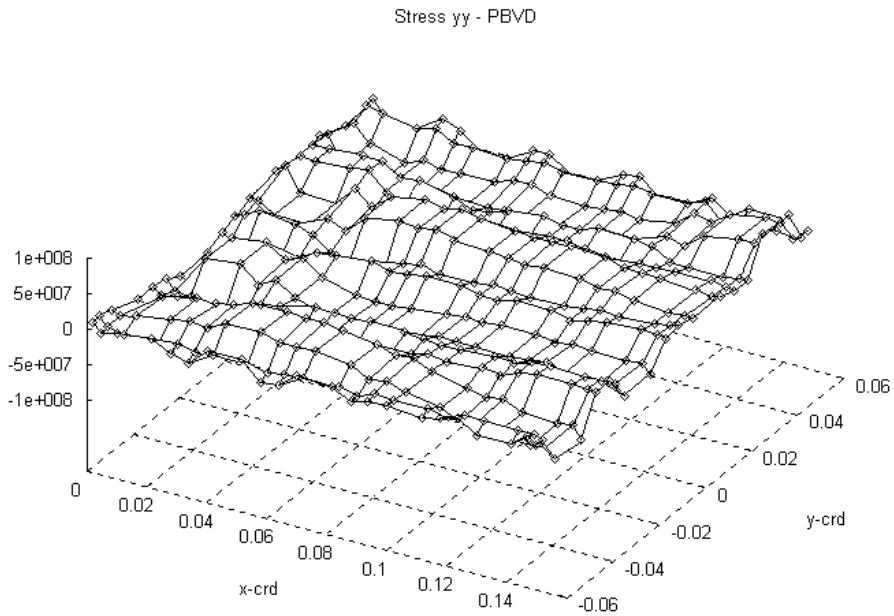

Figure 8.12d. CDSC with PBVD - Stress yy.

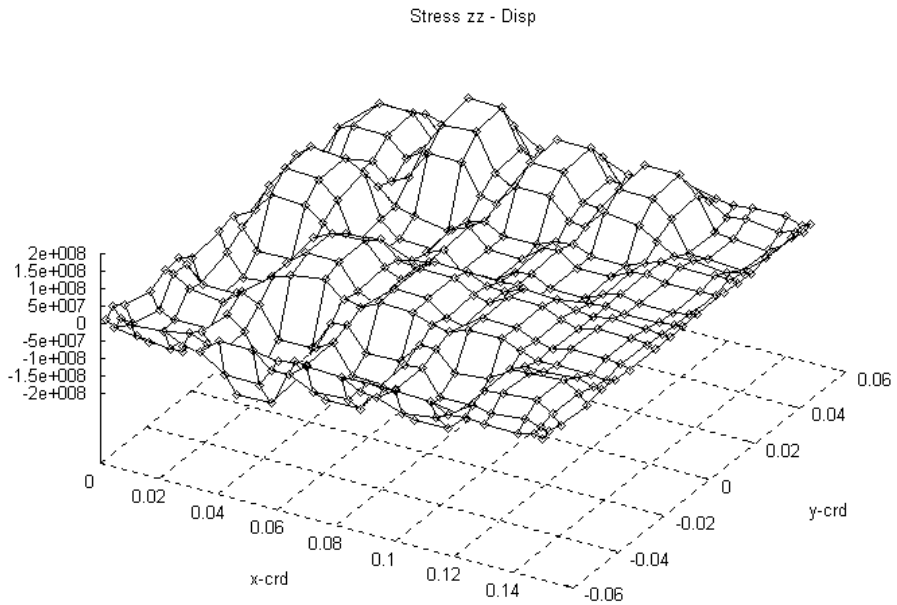

Figure 8.12e. Pure displacement control - Stress zz.

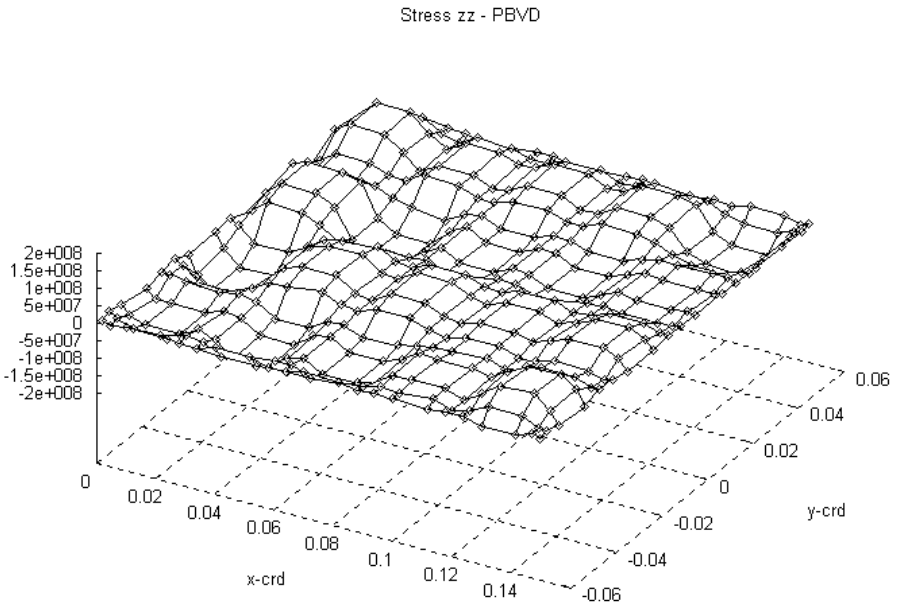

Figure 8.12f. CDSC with PBVD - Stress zz.

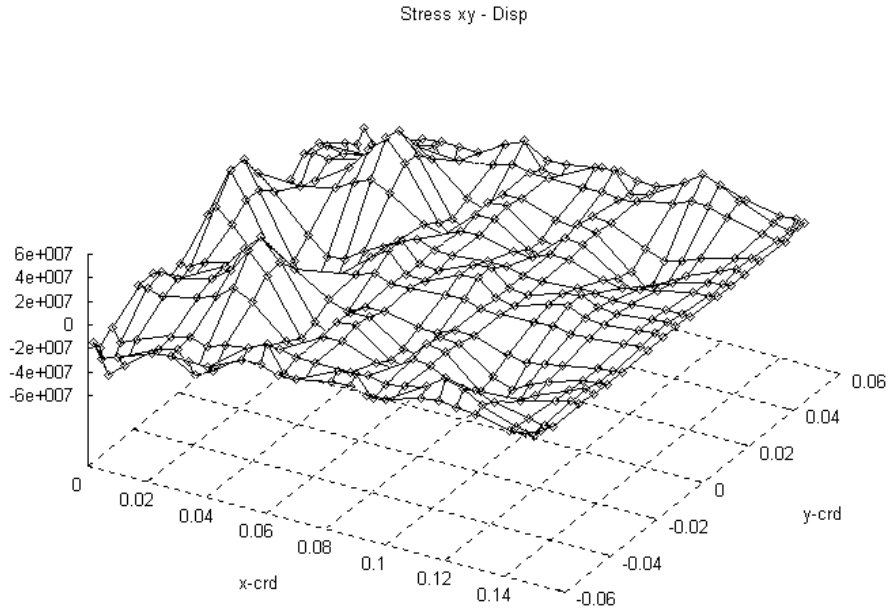

Figure 8.12g. Pure displacement control - Stress xy.

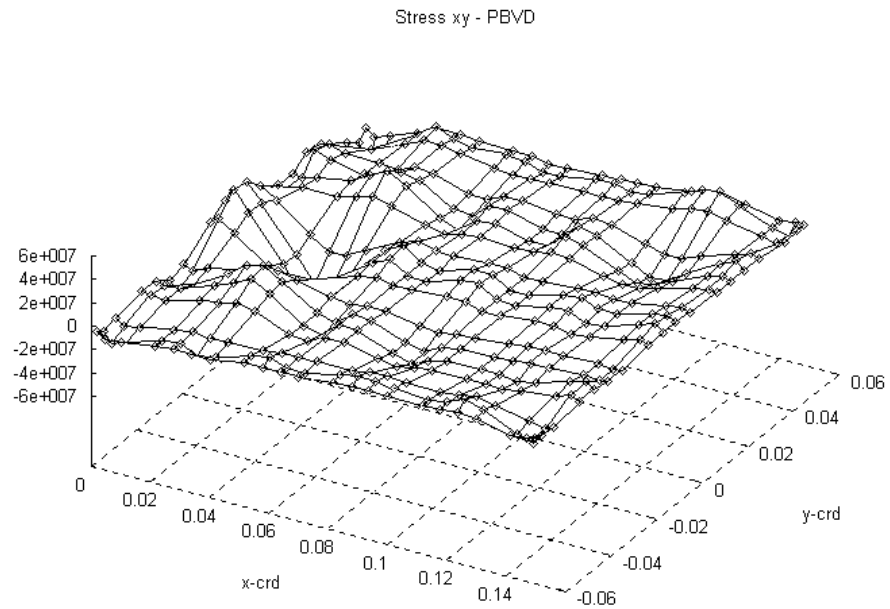

Figure 8.12h. CDSC with PBVD - Stress xy.

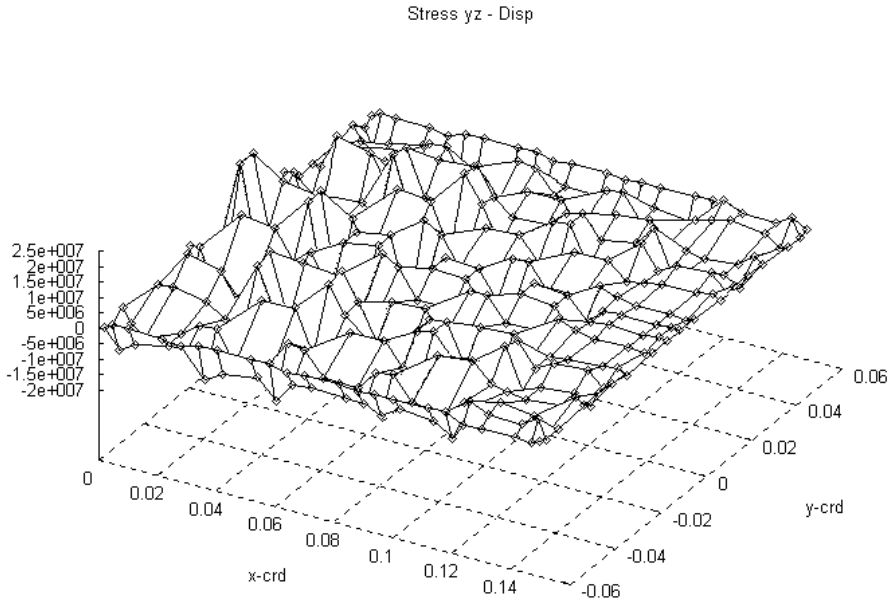

Figure 8.12i. Pure displacement control - Stress yz.

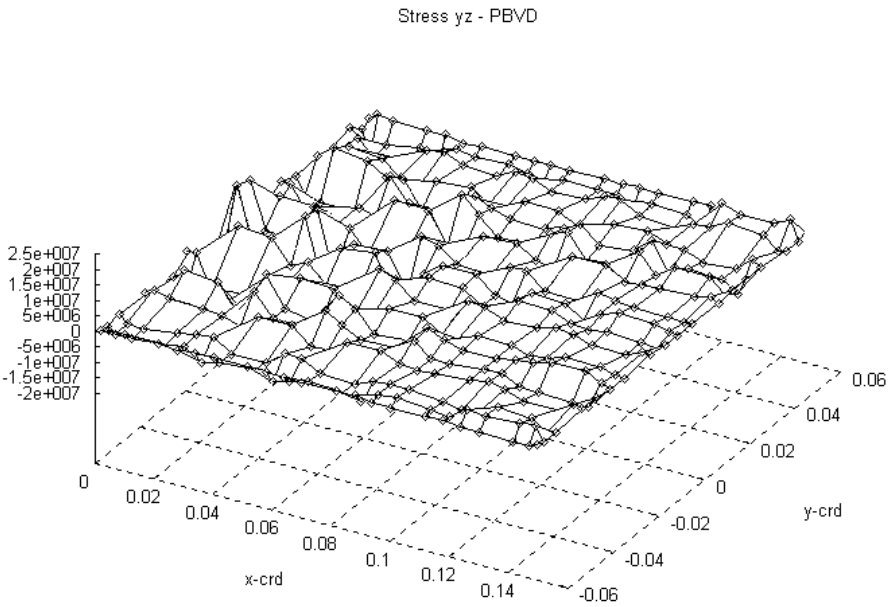

Figure 8.12j. CDSC with PBVD - Stress yz.

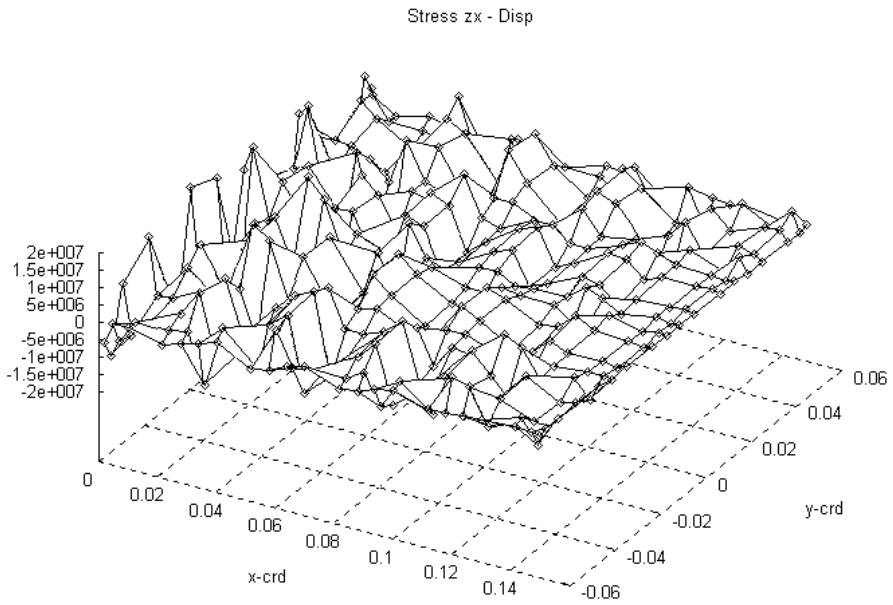

Figure 8.12k. Pure displacement control - Stress zx.

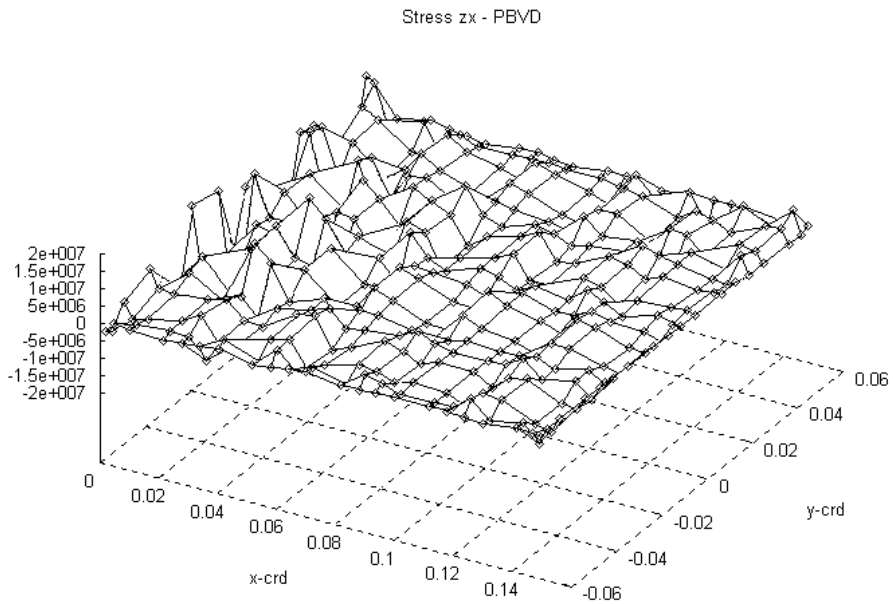

Figure 8.12l. CDSC with PBVD - Stress zx.